We have provided the editor and reviewer comments below in black text with our responses below the comments in blue text. Line numbers in our responses refer to the line numbers in the markup version of the revised text.

Editor Comment:

The uncertainty of the H2O concentration measurements will translate into the uncertainty of CO2 and CH4, which will be significant, however, was not included in the list of systematic uncertainties in Table 2.

The uncertainty in the retrieved water concentration is set by the maximum 10% error in H_2O due to the HITRAN linestrengths. (The typical uncertainty on the H_2O fit is approximately 65 ppm, which is negligible in comparison.) At our ~1% water concentration, this leads to a ~0.1% additional uncertainty in the dry mixing ratios. A row has been added to Table 2 to account for this uncertainty.

Reviewer 1 Comments:

This manuscript, entitled "Intercomparison of Open -Path Trace Gas Measurements with Two Frequency Comb Spectrometers," reports on a quantitative evaluation of atmospheric trace gas measurements based on dual-comb spectroscopy. Thanks to their well-polished dual-comb spectrometers and analytical approach, the retrieved dry mole fractions agree to 0.57 ppm for CO_2 and 7 ppb for CH_4 between the two measurement systems. These results are excellent, while there are some obscure points in the manuscript. Therefore, I recommend the manuscript for publication if following comments and questions are addressed.

We thank Reviewer 1 for taking the time to review this work and for his or her helpful comments.

[Specific comments]

1. While I am briefly familiar with the technique of gas spectroscopy, I am not an expert in atmospheric measurement and concerned about some technical descriptions.

1) Is it OK for AMT readers to use some technical terms such as "WMO-calibration" and "WMO compatibility goal" without any simple explanation?

We have clarified "WMO-calibration" at lines 72-74 which now read "We also compare the DCS retrievals to a cavity ringdown point sensor located near the path that has been tied to the World Meteorological Scale (WMO) manometric scale through calibration with WMO-traceable gases."

The WMO compatibility standards are listed on line 295 with a reference. We have changed the phrase at line 475 to read "WMO compatibility standards" instead of "WMO compatibility goals" to make the language identical.

2) L207: I was confused with the expressions of concentration. Is it correct that dry and wet concentrations of carbon dioxide are expressed as "XCO_2" and "CO_2," respectively?

Yes, the reviewer is correct. We have made no changes at now line 248, however footnote 1 has been modified for clarity on this issue, as noted below.

3) L209: "Volume mole fraction" might be simply "mole fraction."

We agree and have removed the word "volume" at now line 250.

4) Figure 5: I found volume percentage is normally expressed as "v/v%." Is "%v/v" OK too?
We have changed "%v/v" to simply "%" throughout the paper because we are referring to mole fraction rather than volume fraction in this work. We have specifically updated Figure 5 and its caption and Figure 9.

5) According to the footnote in P2, "ppm" and "ppb" are used for dry concentration (dry mole fraction) and "%v/v" is for wet concentration (wet mole fraction) as in Figure 5. However, "ppm" is used for ΔHDO and ΔH_2O in Figure 6 and 7.
We have modified the footnote to clarify that we use ppm and ppb to mean micro or nanomoles of gas per mole of air, and that we specifically mean per mole of dry air when we use XCO_2 or XCH_4. The footnote now reads "We use dry mole fraction for carbon dioxide and methane, denoted respectively as XCO2 in units of ppm, which are micromoles of CO2 per mole of dry air, or XCH4 in units of ppb, which are nanomoles of CH4 per mole of dry air."

6) I think the explanation about dual-comb spectroscopy is a little insufficient. For example,
1) L94 and 97: Authors should refer to Figure 1(a) here instead of Figure 1 and 1(b).
We have rewritten this paragraph and modified Figure 1 in an attempt to convey dual-comb spectroscopy more clearly. We have also separated the more general discussion of dual-comb spectroscopy (now section 2.1) from the more specific instrument discussion (now section 2.3) to try to improve the clarity.

The rewritten paragraph at lines 112-120 reads:
A frequency comb is a laser pulsed at a very precise repetition rate of f_r (Cundiff and Ye, 2003; Hall, 2006; Hänsch, 2006). Because the pulse rate is so precisely controlled, this creates a spectrum consisting of very narrow, evenly-spaced modes called comb teeth. Dual frequency comb spectroscopy combines two of these combs that have very slightly different pulse repetition rates that differ by Δf_r, sends the light through the sample, and on to a detector (see Fig. 1a) (Schiller, 2002; Schliesser et al., 2005; Coddington et al., 2008, 2016; Ideguchi, 2017). It is also possible to transmit only a single comb through the air to measure both dispersion and absorbance (Giorgetta et al., 2015). The basic technique of dual-comb spectroscopy is illustrated in Figure 1 and described in more detail in the literature (Schiller, 2002; Schliesser et al., 2005; Coddington et al., 2008, 2016).

7) L102: I could not understand the explanation "the instrument lineshape is effectively the sum of two delta-functions." What does it mean?
Since both combs pass through the gas, the teeth of both combs are attenuated. These teeth are "delta functions" in frequency as they are very narrow and at precisely known frequencies. The measured signal is the product of the two attenuated teeth, and therefore probes the sample absorption at the two teeth locations. That is what we meant by the sum of the two delta functions. In the reworded Section 2.3 we have added at lines 177-182 "As shown in Fig. 1a, the effective lineshape for each sampled point is well approximated as two closely separated delta-functions located at the known optical frequencies of the two comb lines that are heterodyned to produce the measured rf signal (e.g. consider the solid and dashed yellow optical comb teeth that lead to the single solid yellow rf comb tooth.) The separation of the two delta-functions (comb teeth) is negligible compared to the ~5-GHz wide absorption lines but can be exactly incorporated in the spectral model."

8) L139: Readers might not be sure whether f_r is a sampling rate or bandwidth.
We have clarified this to "digitized at a sampling rate f_r." at now line 171.

9) L183: Please define Cn^2.
We have now defined Cn^2 as the refractive index structure parameter in the text at lines 223-234.

10) In Figure 4, the observed HDO is 10^{-4} %v/v level, whereas ΔHDO is 1000 ppm level in Figure 6 and 7. Are they consistent?
Thank you. The previous figures included a built-in HITRAN isotope scaling factor that we had forgotten to remove. It has now been removed for the HDO concentration. We have also updated the width of the HDO histogram at lines 292-293.

11) In the caption of Figure 8, "40 ppmv/$\sqrt{\tau}$" "4 ppbv/$\sqrt{\tau}$" might be "40 ppm/$\sqrt{\tau}$/s" and "4 ppb/$\sqrt{\tau}$/s," respectively.
The caption now reads "ppm" and "ppb" rather than "ppmv" and "ppbv" and we added "where τ is in seconds".

[Technical corrections]
1. There are some notations without space between the value and unit; for example "1-10s" in L46, "10%" in L51. Please check and correct them.
At line 47, we have changed the text to read "one to tens of kilometers". We have corrected the "10%" to "10 %"at L52 and numerous other instances of this error and additional inconsistencies with the AMT style guide.
2. Notation variability, "dual comb" and "dual-comb."
We have changed all "dual comb" instances to read "dual-comb" (except for one instance that occurred in the references).
3. L94: Reference (Ideguchi, 2017) is missing in the list of references.
We have added this to the reference list at line 563.
4. L214 -215: Notation variability, "three-hour " and "3-hour."
We have corrected to be consistent.
5. L217: A beginning parenthesis is missing.
We have removed the extra).

Reviewer 2 Comments:

This paper compares the performance of two open-path dual comb spectroscopy (DCS) instruments over two weeks and analyzes the measurement differences, also between the DCSs and a Cavity ring down spectrometer measuring in-situ. The paper describes the function principle of the dual comb spectrometers, the optical setup, and the data processing. The precision of the individual DCS is determined using Allan analysis.

This kind of inter-comparison has not been done so far, and the DCS instruments deployed here are novel. The descriptions and analyses are clear structured. The reviewer recommends the publication of this paper, if the following items are addressed.
We thank Reviewer 2 for taking the time to review this work and for his or her helpful comments.

General comments:
1) As the authors noted, the dual comb spectrometer has negligible line width (120 kHz) and high spectral resolution, the absorbance resolution is below 10^{-3} (5×10^{-4}), which is limited by the instrument noise. However, the laser spectroscopic instrument typically has an absorbance resolution of 10^{-5}, limited by the shot noise of the photodiode (also depends on the incoming light intensity). Could the

authors be more specific about the origin of the noise? What kind of instrumental noises are these, photodetector noise, noise from the dual comb laser?
The comparison emphasizes that the two DCS spectra agree to within their instrument noise. This would generally not be the case between laser spectroscopic instruments unless they had precisely the same frequency axis (otherwise one would effectively observe a derivative of the spectrum with higher amplitude than $1e^{-4}$.)

We have added a brief noise discussion in Section 3.1 at lines 259-270 as follows "The difference of the absorption spectra, shown as the black line in Figure 4(c), has a standard deviation of 9×10^{-4} with no observable structure at absorption lines. This difference is dominated by an etalon on the off-axis telescope used with DCS A. After manually fitting out the etalon structure, the remaining difference between DCS A and DCS B is attributed to measurement noise. DCS A has higher return power (see Fig. 3b) and the measurement noise is primarily from relative-intensity noise (RIN) on the comb light. This RIN is mainly white but has a small peak near 14 MHz, which is mapped to ~6290 cm^{-1} in the optical domain, leading to the observed noise increase in that spectral region. DCS B has lower return power and the measurement noise is from the detector. Nevertheless, the two spectra agree to better than 5×10^{-4} over the full spectral region (with the exception of the 7 cm^{-1} section at 6290 cm^{-1}), and better than 2.5×10^{-4} over the region near 6100 cm^{-1} where both DCS systems have significant returned optical power."

2) What benefits in the authors' opinion could be gained from the open-path DCS techniques compared to open path FTIR? There seems to be no benefit in terms of the achievable absorbance resolution, and the measurement precision is comparable. One argument brought by the authors is the "rapid scan rate" and "faster than turbulence-induced intensity variations", and "instrument-specific calibrations" are not needed. In the reviewer's opinion, it would be beneficial if the authors could discuss and summarize the benefits/drawback compared to open path FTIR in one paragraph.
We have followed the reviewer's suggestion and combined the comments on the advantages of DCS into a discussion at the end of the new Section 2.1. We do distinguish between open path FTIR instruments for horizontal column instruments and solar-tracking FTIR instruments that make full vertical column measurements. The open-path horizontal FTIR instruments operate with a resolution of 0.5 to 1 cm^{-1} resolution while the pressure-broadened gas lines are approximately 0.15 cm^{-1} (5 GHz) wide. This leads to the necessity of measuring the instrument lineshape (ILS) and incorporating it into the analysis. On the other hand, DCS measures with a point spacing and instrument lineshape much smaller than the gas absorption lines. The DCS should be much less susceptible to systematics and can even probe the accuracy of spectral models. Other advantages include the collimated laser beam for long distance operation compared to the sub-km range of open path FTS instruments and the insensitivity to turbulence. However, unlike the careful comparisons of solar-looking FTS, it is very challenging to find careful comparisons of open-path FTS in the literature. Indeed, we find no examples of direct horizontal open-path FTS comparisons for greenhouse gases (again as compared to either vertical solar-looking FTS or the data here).

The new paragraph appears at lines 121-138 with the following text:
A DCS system can be thought of as a high-resolution Fourier-Transform spectrometer but has a number of attributes that distinguish it from a conventional horizontal open-path FTS and other open-path instruments that could lead to higher performance atmospheric trace gas monitoring. A compact, mobile DCS system such as this one has no moving parts but dense point spacing (200 MHz or 0.0067 cm^{-1} in this work), effectively no instrument lineshape, and a calibration-free wavelength axis as described in (Rieker et al., 2014; Truong et al., 2016). As a result, it oversamples the 5 GHz-wide (0.15

cm^{-1}) pressure-broadened gas lines of carbon dioxide, methane, water and other small molecules without distortion, which should suppress any instrument-specific systematics and allow comparison of DCS data between instruments and over time. Specifically relevant to open-path measurements, the comb output is a diffraction-limited eye-safe laser beam and can support much longer distances than typical open-path FTS systems; here we demonstrate 2-km round-trip measurements, but we have unpublished data for up to 11.6 km round-trip. Finally, unlike swept laser systems, DCS measures all wavelengths at once rather than sequentially and is therefore much more immune to turbulence effects as described in (Rieker et al., 2014). There are still disadvantages. The current system is not yet turn-key and requires intermittent manual adjustments. The shape of the comb spectrum can vary with wavelength and time, thus requiring a real-time reference to retrieve broad-band molecular absorption lines, and finally the spectral width is narrower than an FTIR. However, none of these disadvantages are fundamental but rather technical challenges to be solved.

3) The principle of dual comb technology should be briefly stated using mathematical formulas, so that it is easier for readers to follow. For example, formulas can be written below "two combs with nominal repetition rates of f_r and offset by Δf_r are phase locked together, transmitted through a sample, and their heterodyne signal measured on a photodetector. The resulting rf frequency comb can be mapped back to the optical domain to generate an overall spectrum".
We have modified Figure 1 and its caption significantly to try to better convey dual-comb spectroscopy. The mathematical formulae are not very helpful compared to this picture but we add explicit references to places where the math is given. (The math requires a more detailed discussion of the comb and its locking conditions, which would be a significant detour for this paper.) We have also modified the discussion of dual-comb spectroscopy, as noted in response to reviewer 1, to separate out the more general description in Section 2.1 from the details of Section 2.3.

4) The authors state that "the instrument line shape is the sum of two Delta impulses as shown in Fig. 1 (b)". The instrument line shape is not visible in Fig. 1 (b). It would be beneficial if the ILS can be schematically shown with the spectral spacing between the two impulses indicated.
We have updated Fig. 1(b) and reworded this discussion as noted in response to reviewer #1 point 7 above.

5. It is difficult to assess the measurement precision of atmospheric open-path instruments because the measurement conditions (P/T/vmr) are usually not stable and constant. The authors use the measurements in 6 hours well-mixed time period to calculate Allan deviations. Can the authors draw any conclusions regarding to the 1000s turning point in the Allan plots? Is it instrument drift or given by variations of the atmospheric conditions?
As discussed in the next point, we have taken up the suggestion of the reviewer and added an Allan deviation of the difference between the instruments. This separates out the atmospheric and instrument variability. As discussed below and in the new wording in Section 3.3, based on this analysis most of the flattening is likely due to the instrument (but only because we have selected a very well-mixed 6 hour period.)

The new text appears at lines 339-346 and states:
As in (Chen et al., 2016) it is also useful to plot the Allan deviation of the difference in retrieved concentration between the instruments, e.g. ΔXCO_2 and ΔXCH_4 of Figure 6. This removes the atmospheric variability from the Allan deviation and provides information on the relative stability of the two instruments. As it includes contributions from both DCS instruments, it lies above both individual Allan deviations but similarly reaches a floor at ~1000 s, indicating the floor of the individual Allan

deviations is likely dominated by instrument rather than atmospheric variability for these data. We note a similar floor is found in (Truong et al., 2016) for static laboratory cell data where it was attributed to the existence of an etalon.

6. The authors have done Allan analysis to assess the precision of individual DCS. The reviewer thinks that it would be interesting to conduct the Allan analysis for the measured concentration differences (Fig. 6). On one hand, it will give an indication of the precision of the differential measurements, on the other hand, the atmospheric influences will be cancelled out, which could be advantageous for conducting Allan analysis. Differential column measurements have been recently successfully used for determining local/city emissions [1, 2]. In [1] the measured differences between two side-by-side solar-viewing FTIRs are analyzed using Allan analysis, to determine the precision of the differential system that consists of two spectrometers (0.01% for XCO2 and XCH4 over 10-minute integration time) and the precision of an individual instrument (assuming the instruments are the same and the measurement noises are statistically uncorrelated). [1] presents a new way to determine the precision of atmospheric measurements, and could be included in the references.
We agree and have added Allan deviation of the differences of XCO_2 and XCH_4 to the new Figure 8 along with a reference to [1] of the reviewer comments. As suggested, it is useful to examining both the individual and differential Allan deviations since it clarifies that most of the "flattening" at 1000s is likely due to instrument effects rather than atmospheric variability.

We have left Figure 7 that shows the histogram of the differences because it conveys both the precision at a particular time (via the width) and the absolute difference (via the center position) between the retrieved concentrations. A potential strength of DCS is that there is no instrument-specific calibration and it was important to quantify whether the two instruments retrieved the same concentration; the Allan deviation does not capture that. In other words, one could measure a very low Allan deviation but still have a very large offset between instruments.

7. Statistical distribution of the differences (caption of Fig. 7): if the Allan deviation of the differences follows a square root law (inversely proportional to the square root of the integration time), the distribution widths should be the third when increasing the integration time from 32s to 5 min (factor 10).
Yes, we agree and the broader width at 5 min reflects the instrument drift at that time scale. As the reviewer suggested in the previous comment, this effective floor with averaging time is captured best in the Allan deviation that has been added to Figure 8. (See answer to comment above.)

Specific comments:
1. Line 16: better to write "5×10^{-4} in absorbance"
We have made this change.
2. Line 17: better to write "path-integrated concentrations for carbon dioxide (CO2)"
We have made this change.
3. Line 19: averaging time interval information is missing: at 32 s integration time
We have made this change (now at line 20).
4. Line 125: "with nominal repetitions rates f_r and the difference in the repetition rates Δf_r"
We have made this change (now at line 159).
5. Line 132: absolute frequency accuracy is written in wavenumber, it would be beneficial if it is also converted to frequency, i.e. 1 MHz.
We have made this change (now at line 164).

6. Line 220: which parallel surfaces cause these etalons?
It is unclear (or we would remove them). They could be in one of the fiber-optic components or in the free-space optics. We have removed as many etalons as possible in the design but since we do not know the origin of these, we have not speculated.

7. Fig. 4: big discrepancies around 6290 cm^{-1} in both (c) the differences between absorption spectra and (d) fitting residual, please specify the reason for it.
This noise originates from excess laser noise on one of the systems that is related to the use of semiconductor saturable absorber mirror (SESAM) (see Sinclair et al. (2015) Rev. Sci. Inst. for further details). The noise appears at ~14 MHz in the RF domain, but is scaled up to the optical along with the rest of the RF comb, ending up at ~188 THz/6290 cm^{-1}.
Section 3.1 now has the added words that explain this noise as discussed in point 1 above.

8. Line 644, caption of Fig. 8: ...highlighted in Fig. 3 -> it should be Fig. 5
Thank you, we have fixed this.

References cited by the authors:
Coddington, I., Newbury, N. and Swann, W.: Dual-comb spectroscopy, Optica, 3(4), 414, doi:10.1364/OPTICA.3.000414, 2016.

Sinclair, L. C., Deschênes, J.-D., Sonderhouse, L., Swann, W. C., Khader, I. H., Baumann, E., Newbury, N. R. and Coddington, I.: Invited Article: A compact optically coherent fiber frequency comb, Rev. Sci. Instrum., 86(8), 081301, doi:10.1063/1.4928163, 2015.

Truong, G.-W., Waxman, E. M., Cossel, K. C., Baumann, E., Klose, A., Giorgetta, F. R., Swann, W. C., Newbury, N. R. and Coddington, I.: Accurate frequency referencing for fieldable dual-comb spectroscopy, Opt. Express, 24(26), 30495, doi:10.1364/OE.24.030495, 2016.

Intercomparison of Open-Path Trace Gas Measurements with Two Dual Frequency Comb Spectrometers

Eleanor M. Waxman[1], Kevin C. Cossel[1], Gar-Wing Truong[1], Fabrizio R. Giorgetta[1], William C. Swann,[1]
Sean Coburn[2], Robert J. Wright[2], Gregory B. Rieker[2], Ian Coddington,[1] and Nathan R. Newbury[1]
[1]Physical Measurement Laboratory, National Institute of Standards and Technology, 325 Broadway, Boulder, CO 80305
[2]Precision Laser Diagnostics Laboratory, University of Colorado Boulder, Boulder, CO 80309
Correspondence to: Eleanor Waxman
(eleanor.waxman@nist.gov)

Abstract

We present the first quantitative intercomparison between two open-path dual comb spectroscopy (DCS) instruments which were operated across adjacent 2-km open-air paths over a two-week period. We used DCS to measure the atmospheric absorption spectrum in the near infrared from 6021 to 6388 cm^{-1} (1565 to 1661 nm), corresponding to a 367 cm^{-1} bandwidth, at 0.0067 cm^{-1} sample spacing. The measured absorption spectra agree with each other to within 5×10^{-4} in absorbance without any external calibration of either instrument. The absorption spectra are fit to retrieve path-integrated concentrations for carbon dioxide (CO_2), methane (CH_4), water (H_2O), and deuterated water (HDO). The retrieved dry mole fractions agree to 0.14 % (0.57 ppm) for CO_2, 0.35 % (7 ppb) for CH_4, and 0.40 % (36 ppm) for H_2O at ~30-second integration time over the two-week measurement campaign, which included 23 °C outdoor temperature variations and periods of strong atmospheric turbulence. This agreement is at least an order of magnitude better than conventional active-source open-path instrument intercomparisons and is particularly relevant to future regional flux measurements as it allows accurate comparisons of open-path DCS data across locations and time. We additionally compare the open-path DCS retrievals to a WMO-calibrated cavity ringdown point sensor located along the path with good agreement. Short-term and long-term differences between the ~~two systems~~open-path DCS and point sensor are attributed, respectively, to spatial sampling discrepancies and to inaccuracies in the current spectral database used to fit the DCS data. Finally, the two-week measurement campaign yields diurnal cycles of CO_2 and CH_4 that are consistent with the presence of local sources of CO_2 and absence of local sources of CH_4.

1. Introduction

Quantitative determination of greenhouse gas fluxes over a variety of temporal and spatial scales is necessary for characterizing source strength and intermittency and for future emissions monitoring, reporting, and verification. To this end, techniques exist to measure greenhouse gas concentrations on a variety of length scales, each of which has advantages and disadvantages. Point sensors provide valuable information about local sources, but their use for continuous regional measurements on sampling towers is complicated by local wind patterns, local sources, and mixing within the planetary boundary layer (PBL), especially at night (Lauvaux et al., 2008; Ciais et al., 2010; Lauvaux et al., 2012). Similarly, total-column measurements are particularly useful for sub-continental to global scale measurements; however they are sensitive to atmospheric transport errors within the PBL (Lauvaux and Davis, 2014), are affected by clouds and aerosols, are primarily limited to daytime measurements, and lack either the revisit rates or mobility for regional flux measurements. Horizontal integrated path measurements are complementary to point sensors and satellites: they cover spatial scales from ~~1-10s~~one to tens of kilometers and provide measurements on the second to minute time scales with portable instruments and are thus appropriate for regional studies. Active-source open-path

sensors such as open-path Fourier Transform Infrared spectroscopy (FTIR), differential optical absorption spectroscopy (DOAS), differential LIDAR (DIAL), or tunable diode laser absorption spectroscopy (TDLAS) are often used for these measurements and can retrieve path-averaged concentrations but typically with 10 % or greater uncertainties (EPA Handbook, and references therein). Recently, open-path dual-comb spectroscopy (DCS) has emerged as a new technique that could potentially provide precise, accurate continuous regional measurements of the mole fractions of CO_2, CH_4, H_2O, and HDO over kilometer-scale open paths (Rieker et al., 2014), thereby providing a new open-path sensing capability that falls between point sensing and total-column measurements.

Here we demonstrate that open-path DCS can indeed yield dry mole fractions over open-air paths with a high level of intercomparibility, over long periods of time, and with sufficient precision to track variations in the ambient levels from local sources and sinks. Two completely independent open-path DCS instruments are operated over neighboring open-air paths during a ~~two-~~2 week measurement campaign. Although both DCS instruments use fully stabilized frequency combs, they are portable (Truong et al., 2016) and are operated nearly continuously during both day and night through laboratory temperature variations from 17 to 25 °C, strong atmospheric turbulence, and outdoor air temperature variations from 4.6 to 28.9 °C. The retrieved dry mole fractions for the two DCS instruments agree to better than 0.57 ppm[1] (0.14 %) for CO_2 and 7.0 ppb (0.37 %) for CH_4. This agreement is achieved without any "bias correction" or calibration of either instrument for absolute wavelength or for absolute concentration. Instead, it is a direct consequence of the negligible instrument lineshape and precise frequency calibration of the DCS instruments, which leads to measured atmospheric absorption spectra that are identical to below 10^{-3} and as low as 2.5×10^{-4} (limited by the instrument noise level). The measured path-averaged CO_2 precision over a ~~2 km~~2km path is 0.90 ppm in 30 seconds, improving to 0.24 ppm in 5 minutes. For CH_4, the precision is 9.6 ppb in 30 seconds, improving to 2.1 ppb in 5 minutes. We also compare the DCS retrievals to a ~~WMO-calibrated,~~ cavity ringdown point sensor located near the path that has been tied to the World Meteorological Scale (WMO) manometric scale through calibration with WMO-traceable gases. The agreement is within 3.4 ppm and 17 ppb for CO_2 and CH_4 respectively, limited by differences in the sampling volume and by the spectral database used to analyze the DCS transmission spectra.

Similar intercomparison measurements between conventional active, open-path sensors are rare but have shown agreement of typically 1-20 % (Thoma et al., 2005; Hak et al., 2005; Smith et al., 2011; Shao et al., 2013; Conde et al., 2014; Reiche et al., 2014; Thalman et al., 2015). Here, we find agreement between two DCS instruments that is an order of magnitude better and is comparable to that achieved with highly-calibrated, state-of-the-art, solar-looking FTIRs that retrieve vertical column measurements (Messerschmidt et al., 2011; Frey et al., 2015; Hedelius et al., 2016); however, open-path DCS does not require instrument-specific calibrations (e.g. of the instrument line shape) and provides a very different capability by retrieving the dry mole fractions across regional, kilometer-scale paths over day and night in a mobile platform. Moreover, as the agreement between open-path DCS instruments is below the level of natural background fluctuations, future measurements can facilitate accurate inverse modeling to identify sources and sinks of carbon emission over regions. As an initial demonstration, we discuss the observed diurnal variations from this two-week measurement campaign in the final section of the paper.

2 Technique

2.1 ~~Overview~~Dual-Comb Spectroscopy

[1] ~~In this work we~~We use dry mole fraction~~. ppm is defined~~ for carbon dioxide and methane, denoted respectively as XCO_2 in units of ppm, which are micromoles of CO_2 per mole of dry air~~ and~~, or XCH_4 in units of ppb~~ is defined as~~, which are nanomoles of CH_4 per mole of dry air.

~~DCS is based on a frequency comb laser source, which is a pulsed laser that outputs a spectrum consisting of evenly-spaced, narrow modes ("comb teeth") underneath a broad spectral envelope (Cundiff and Ye, 2003; Hall, 2006; Hänsch, 2006). In DCS, two such frequency combs are used to measure the atmospheric absorption on a comb-tooth-by-tooth basis across broad bandwidths (Coddington et al., 2016; Ideguchi, 2017). As shown in Figure 1, two combs with nominal repetition rates of f_r and offset by Δf_r are phase locked together, transmitted through a sample, and their heterodyne signal measured on a photodetector. The resulting rf frequency comb can be mapped back to the optical domain to generate an overall spectrum, as shown in Figure 1(b), that is the product of the comb spectra and any atmospheric absorption. One important difference between DCS and other broad-band laser techniques is that here all wavelengths are measured at once rather than sequentially as would be the case for a swept laser system; as a result, DCS is much more immune to spectral distortions from turbulence effects. Moreover, for a fully phase-locked comb, as is used here, the optical frequency axis is stable and known to high accuracy, and the instrument lineshape is effectively the sum of two delta-functions, as shown in the spectrum in Figure 1(b). Alternatively, DCS can be thought of as high-resolution Fourier-transform spectroscopy with diffraction-limited light sources, no moving parts, negligible instrument line shape, and a rapid scanning rate of $1/\Delta f_r$, which we tune to be faster than turbulence-induced intensity variations. Here, both combs are transmitted over the open path yielding the atmospheric absorption spectrum, but it is also possible to transmit only a single comb through the air to measure both dispersion and absorbance (Giorgetta et al., 2015; Coddington et al., 2016).~~

A frequency comb is a laser pulsed at a very precise repetition rate of f_r (Cundiff and Ye, 2003; Hall, 2006; Hänsch, 2006). Because the pulse rate is so precisely controlled, this creates a spectrum consisting of very narrow, evenly-spaced modes called comb teeth. Dual frequency comb spectroscopy combines two of these combs that have very slightly different pulse repetition rates that differ by Δf_r, sends the light through the sample, and on to a detector (see Fig. 1a) (Schiller, 2002; Schliesser et al., 2005; Coddington et al., 2008, 2016; Ideguchi, 2017). It is also possible to transmit only a single comb through the air to measure both dispersion and absorbance (Giorgetta et al., 2015). The basic technique of dual-comb spectroscopy is illustrated in Figure 1 and described in more detail in the literature (Schiller, 2002; Schliesser et al., 2005; Coddington et al., 2008, 2016).

A DCS system can be thought of as a high-resolution Fourier-Transform spectrometer but has a number of attributes that distinguish it from a conventional, horizontal open-path FTS and other open-path instruments, which ~~that~~ could lead to higher performance atmospheric trace gas monitoring. A compact, mobile DCS system such as this one has no moving parts, ~~but~~ dense point spacing (200 MHz or 0.0067 cm^{-1} in this work), effectively no instrument lineshape, and a calibration-free wavelength axis as described in (Rieker et al., 2014; Truong et al., 2016). As a result, it oversamples the 5 GHz-wide (0.15 cm^{-1}) pressure-broadened gas lines of carbon dioxide, methane, water and other small molecules without distortion, which should suppress any instrument-specific systematics and allow comparison of DCS data between instruments and over time. Specifically relevant to open-path measurements, the comb output is a diffraction-limited eye-safe laser beam and thus can support much longer distances than typical open-path FTS systems; here we demonstrate 2-km round-trip measurements, but we have unpublished data for up to 11.6 km round-trip. Finally, unlike swept laser systems, DCS measures all wavelengths at once rather than sequentially and is therefore much more immune to turbulence effects as described in (Rieker et al., 2014). However, t~~T~~here are still disadvantages. The current system is not yet turn-key and requires intermittent manual adjustments. The shape of the comb spectrum can vary with wavelength and time, thus requiring a real-time reference to retrieve broad-band molecular absorption lines, and finally the spectral ~~width~~coverage is ~~narrower~~smaller than an FTIR. However, none of these disadvantages are fundamental but rather technical challenges to be solved.

2.2 Overview of experiment

Figure 2 provides an overview of our experiment. Two DCS instruments measured the atmospheric absorption across a ~~2-km-roundtrip~~2-km round-trip open path that extended from the top of a building at the National Institute of Standards and Technology (NIST) Boulder campus to a pair of retroreflectors located on a nearby hill. Both DCS instruments were based on a similar overall design and used self-referenced, stabilized frequency combs (Sinclair et al., 2015), but one was built by a team at NIST and the other by a team at the University of Colorado; they are hereafter referred to as DCS A and DCS B, respectively. As outlined below, the two instruments differed in their exact design and physical parameters. Nevertheless, no instrument-specific calibration or bias offset was applied to either system. The acquired atmospheric absorption spectra were fit to retrieve the column density of CO_2, CH_4, and H_2O (as well as HDO and $^{13}CO_2$ at lower precision) along with the path-averaged temperature from the CO_2 spectrum. From these data, combined with the measured atmospheric pressure and the path length (measured via time-of-flight laser ranging), we retrieved the path-averaged dry mole fractions as a function of time, which are compared between DCS instruments and to a nearby cavity ringdown (CRDS) point sensor.

2.~~2~~3 Dual comb spectrometer

Figure 3(a) shows a simplified schematic of both DCS setups. Briefly, each DCS system used two mutually coherent self-referenced erbium-doped fiber frequency combs based on the design of (Sinclair et al., 2015) with nominal repetitions rates f_r and the difference in repetition rates Δf_r given in Table 1. Mutual optical coherence between the combs is enforced by phase-locking an optical tooth of each to a common cw laser and the carrier-envelope offset frequency of each to a common quartz microwave oscillator. Absolute frequency accuracy is then enforced by a bootstrapped approach that effectively locks the common cw laser to the same quartz microwave oscillator (Truong et al., 2016). The result is sub-Hz mutual coherence, ~~120-kHz~~120kHz (4×10^{-6} cm^{-1}) absolute linewidths, and 1.1 MHz (3.6×10^{-5} cm^{-1}) absolute frequency accuracy (Truong et al., 2016)~~. This linewidth is orders of magnitude lower than the ~5 GHz or ~0.2 cm^{-1} width of pressure-broadened absorption lines.~~. The direct output of the combs is spectrally broadened in highly nonlinear fiber to cover 7140-5710 cm^{-1} (1.4-1.75 μm) and then filtered to isolate the spectral region of interest from 6021 to 6388 cm^{-1} (1565 to 1661 nm).

The combined light from both combs is transmitted via single-mode fiber to a telescope, where it is launched to a retroreflector. The returning signal is collected onto an amplified, ~~100-MHz~~ 100MHz bandwidth InGaAs photodetector and digitized at a sampling rate f_r. We acquire a single interferogram at a period of $1/\Delta f_r$ or 1.6 ms for DCS A; 100 such interferograms are directly summed in real time on a field-programmable gate array (FPGA). These are transferred to a computer where they are carrier-phase corrected and further summed over an acquisition time of ~30 seconds. These summed interferograms are then Fourier transformed and scaled, using the known optical frequency comb tooth positions, to generate a transmission spectrum (e.g. Figure 4a) spanning 367 cm^{-1} (>10 THz) with a point spacing of 0.0067 cm^{-1}. As shown in Fig. 1a, the effective lineshape for each sampled point is well approximated as two closely separated delta-functions located at the known optical frequencies of the two comb lines that are heterodyned to produce the measured rf signal (e.g. consider the solid and dashed yellow optical comb teeth that lead to the single solid yellow rf comb tooth.) The separation of the two delta-functions (comb teeth) is negligible compared to the ~5-GHz wide absorption lines but can be exactly incorporated in the spectral model.

The exact optical layout of DCS A is given in (Truong et al., 2016). While following the same basic design, DCS B differs in several technical details. These include a slightly different output spectrum, as well as slight different comb tooth spacings and offset frequency, minor differences in the reference cw laser and its locking scheme, and different amplifier design, launched and received powers, and telescope design. Some of these differences are laid out in Figure 3, Table 1, and Section 2.~~3~~4 below.

We have found that the use of stabilized, phase coherent frequency combs is a necessary but not sufficient prerequisite to reaching sub-percent agreement in retrieved gas concentrations. It is critical that the spectrally-filtered comb output does not include stray unfiltered light. Similarly, any stray reflections from the telescope that can "short circuit" the atmospheric path must be avoided. As with FTIR systems, nonlinearities are problematic. In the optical domain, nonlinearities can arise when the combs are combined in fiber with high optical power. These are minimized for DCS A by filtering the light, which decreases the peak powers, before combining the combs. For DCS B the combs do not have a booster amplifier and thus have significantly lower power. Nonlinearities in the photodetection can also occur (Zolot et al., 2013); in laboratory tests with a CO reference cell, we verified no bias in retrieved concentration as a function of received power up to 300 μW, which is a factor of two higher than the maximum power for the open path data. It was also critical to match the interferogram amplitude to the full dynamic range of the analog-to-digital converters (ADCs) to avoid effective nonlinearities in the digitization process.

2.~~3~~4 Launch/Receive telescope

The two telescope systems are shown in Figure 3(a). Due to the large spectral bandwidth, reflective optics are preferred to minimize chromatic dispersion. For DCS A, the launch/receive system was based on a bi-directional off-axis parabolic telescope with a 3" aperture while for DCS B, it was based on a 6"-aperture Ritchey-Chretien (RC) telescope with the light launched separately from behind the secondary mirror. In both cases, the launched beam diameter was ~ 40 mm and the light was directed to a hollow corner-cube retroreflector of 2.5" (DCS A) or 5" (DCS B) diameter. A slow servo was implemented for long-term pointing of the telescope to the retroreflectors. For this servo, a low-divergence 850 nm LED is co-aligned with the telescope and its retro-reflected light is detected by a co-aligned CMOS camera with a long focal-length lens and an 850-nm-bandpass optical filter. We then servo the overall telescope pointing via its gimbal using the LED spot location on the camera. ~~Further servo details are described in Cossel et al. (2017).~~Further servo details are described in (Cossel et al., 2017).

Figure 3(b) shows the return power for both systems as a function of time. For reference, the minimum return power required to obtain useful spectra was ~15 μW (horizontal black line). At lower powers, the acquired individual spectra are excluded. Turbulence-induced intensity variations are lower for the RC-telescope than the off-axis parabolic telescope because of its larger aperture; however, the long-term stability of the off-axis parabolic telescope was better due to a higher-quality gimbal system. The collection efficiency of the 6" RC telescope system was about 10-20~~% in low to moderate turbulence (C_n^2 of 10^{-14}). The collection efficiency of the off-axis parabolic telescope system was lower, at ~ 2-4~~ % in low to moderate optical turbulence (C_n^2 of 10^{-14} $m^{2/3}$, where C_n^2 is the refractive index structure parameter and is a measure of optical turbulence (Fante, 1975)). The collection efficiency of the off-axis parabolic telescope system was lower, at ~ 2-4 % in similar conditions, due to 1) the smaller collection aperture and 2) the 50:50 beam splitter, which causes a factor of 4 loss. Attempts to replace the 50:50 splitter with a polarizing beam splitter and quarter-wave plate combination increased the collection efficiency but introduced additional etalons across the spectrum and for this reason was not used.

2.~~4~~5 Data processing

The acquired transmission spectra are the product $S(\nu) = I_0(\nu) \times e^{-A(\nu)}$, where I_0 is the geometric mean of the two individual comb spectra, $A(\nu)$ is the desired atmospheric absorbance, and ν is the average optical frequency of the two participating comb teeth, (e.g. Fig. 1(b)). We fit the natural logarithm of the transmission spectra, $-\ln[S(\nu)] = -\ln[I_0(\nu)] + A(\nu)$, where the first term is represented by a piecewise polynomial and the second by an absorption spectrum calculated from a spectral database with floated concentrations of $^{12}CO_2$, $^{13}CO_2$, $^{12}CH_4$, $^{13}CH_4$, H_2O, and HDO. For a spectral

database we use HITRAN 2008 (Rothman et al., 2009) and Voigt lineshapes as this generates a consistent set of line parameters across our conditions and gases. The fit is performed in three steps: first, we fit the polynomial (typically ~~7th~~seventh order) over small windows (typically 100 GHz or 3.33 cm^{-1}) and include the expected absorbance from relevant gas absorption lines. These polynomials are then stitched together to generate the overall polynomial baseline, which is removed from the measured spectrum to find $A(v)$. We then fit only the 30013 ← 00001 CO_2 band in order to retrieve the path-averaged temperature. Finally, $A(v)$ is then re-fit over the entire spectral window by floating the gas concentrations at the retrieved path-averaged temperature. The retrieved path-averaged concentrations are converted to wet mole fractions by normalizing to the total number density of air molecules, which is calculated from the fitted (or separately measured) air temperature combined with the atmospheric pressure, as measured by a sensor co-located with the CRDS sensor and corrected for the altitude difference. Finally, wet CO_2, $^{13}CO_2$, and CH_4 are converted to dry values (XCO_2, $X^{13}CO_2$, XCH_4) using $XS = S/(1-c_{H2O})$ where XS is the dry species ~~concentration~~mixing ratio, S is the retrieved wet species ~~concentration~~mixing ratio and c_{H2O} is the retrieved H_2O ~~volume~~ mole fraction.

3 Intercomparison Results and Discussion

3.1 Atmospheric spectrum comparison

Figure 4(a) shows the overall raw DCS transmission spectra from the two instruments averaged for a ~~three-hour~~3h period. They differ significantly because of the different comb intensity profiles, $I_0(v)$. However, after the polynomial baseline fit discussed above is applied, the resulting ~~3-hour~~3h averaged absorption spectra are nearly identical as shown in Figure 4(b). The inset of Figure 4(b) shows the data sampling points (spaced at ~200 MHz) across several absorption lines with width of 5 GHz 0.2 cm^{-1}~~),~~, indicating we have sufficient optical resolution to over-sample the lines. The difference of the absorption spectra, shown as the black line in Figure 4(c), has a standard deviation of 9×10^{-4} with no observable structure at absorption lines. This difference is dominated by an etalon on the off-axis telescope used with DCS A. After manually fitting out the etalon structure, the remaining difference between DCS A and DCS B is attributed to measurement noise. DCS A has higher return power (see Fig. 3b) and the measurement noise is primarily from relative-intensity noise (RIN) on the comb light. This RIN is mainly white but has a small peak near 14 MHz, which is mapped to ~6290 cm^{-1} in the optical domain, leading to the observed noise increase in that spectral region. DCS B has lower return power and the measurement noise is from the detector. Nevertheless, the two spectra agree to better than 5×10^{-4} ~~(limited by the instrumental noise level)~~ over the full spectral region (with the exception of ~~a~~the 7 cm^{-1} section at 6290 cm^{-1}), and better than 2.5×10^{-4} over the region near 6100 cm^{-1} where both DCS systems have significant returned optical power. This very high level of agreement between the two spectra shows that there are no instrumental line shapes or detector nonlinearity effects distorting the observed spectral line shapes; otherwise, structure would be observed in the difference. ~~-~~Thus, the two DCS instruments measure the same comb-tooth-resolved atmospheric absorbance spectrum.

Figure 4(d) shows the residuals after fitting the absorption lines in the DCS A spectrum to HITRAN 2008 and removing the etalon. The higher SNR of the DCS A yields an even lower broadband noise than the difference spectrum, but there are clear residuals near spectral lines attributable to incorrect line shapes/parameters in the HITRAN 2008 database. Nevertheless, the overall magnitude of the residuals is very small in comparison to the spectral absorption.

3.2 Comparison of retrieved mole fractions from DCS A and DCS B

From the fitted concentrations, we retrieve the mole fractions as outlined in Section 2.~~4~~5. The retrieved time series for XCO_2, $X^{13}CO_2$, XCH_4, H_2O, and HDO are given in Figure 5 at ~30 second intervals. Gaps in the data are due to either telescope misalignment (primarily on the 6" RC telescope due to the lower-quality gimbal system) or, more rarely, a loss of phase lock of one of the four frequency combs.

Excellent agreement is observed between both systems for all retrieved concentrations. Figure 6 shows the concentration differences, which exhibit a high-frequency white noise consistent with the quadrature sum of the DCS precisions given in Section 3.3. In addition, the differences show a slow wander about zero indicating slowly changing, small offsets between the two DCS instruments. CH_4 also shows a small negative offset for the second week of the campaign. A Gaussian curve approximates the distribution of the differences over the full two weeks reasonably well and is shown in Figure 7. At 32-second averaging times, the mean and width of the distributions are $\Delta XCO_2 = 0.57 \pm 2.4$ ppm, $\Delta XCH_4 = -7.0 \pm 16$ ppb, $\Delta c_{H2O} = 36 \pm 90$ ppm, and $\Delta c_{HDO} = 390 \pm 8600.10 \pm 0.30$ ppm. These widths decrease to 1.5 ppm, 12 ppb, 66 ppm, and 4800.17 ppm, respectively, for 5-minute5minute averaging times. These mean values correspond to a relative offset of 0.14 % CO_2, -0.35 % CH_4, and 0.4 % H_2O and are close to the WMO compatibility standards of 0.1 ppm for CO_2 and 2 ppb for CH_4 (Tans and Zellweger, 2015). We emphasize the agreement here is achieved over a two-week period despite outdoor temperature variations of 4.6 to 28.9 °C, DCS instrument ambient temperature variations from 17 to 25 °C, 10 % to 90 % relative humidity fluctuations, and large turbulence-induced return power fluctuations.

Table 2 summarizes the systematic uncertainties of the DCS systems. The choice of spectral model effectively sets the calibration that converts the measured absorbance spectrum to path-averaged concentrations. The temperature primarily affects the conversion of the path-averaged concentration to mole fractions (through the calculation of the overall air concentration). For the direct intercomparison, both DCS data were analyzed with a common spectral model (HITRAN 2008) and temperature in order to separate out instrument-specific systematics from the more fundamental connection between absorption and concentration. Below we discuss these instrument-specific systematics (given in the top part of Table 2). A discussion of the uncertainties from the spectral model and temperature (given in the bottom part of Table 2) is given in Section 3.5. in terms of instrument-specific systematics in the top of the table, and model-dependent uncertainties common to both instruments in the bottom part of the table. We discuss the instrument-specific uncertainties below and the model-dependent uncertainties in Section 3.5 in the context of the comparison with the point sensor.

To explore the source of the small systematic offsets between the DCS retrievals, we have performed a number of control comparisons. In the processing, we have varied the initial concentration guess in the fit with negligible effect. We have also varied the polynomial baseline fit by adjusting the window size from 100 to 150 GHz and polynomial order from 7thseventh to 9thninth order and again found negligible variations of 0.02 % for CO_2 (<0.07 ppm), 0.07 % for CH_4 (<1.4 ppb), and 0.05 % (~4 ppm) for H_2O. In laboratory tests, we verified that the two DCS instruments retrieve the same CO_2 concentrations to within 0.04 % for 8450 ppm of CO_2 in a 30-meter30m multipass cell (roughly mimicking the total absorption over the open path). In open-path tests, we have separated effects of the detection/acquisition system and optical system. First, the detected DCS A return signal was split to the two separate data acquisition systems. The two processed signals yielded small differences of 0.16 ppm CO_2, 0.34 ppb CH_4, and 1.0 ppm H_2O, presumably due to residual nonlinearities and reflections in the rf system and digitization. Second, the outgoing DCS A comb light was split and directed to the two different telescopes and acquisition systems. These two processed signals yielded larger differences of 0.45 ppm CO_2, 1.5 ppb CH_4, and 56 ppm H_2O, possibly due to scattered light or polarization dependences in the launch and receive optical systems. Finally, residual phase noise between the two combs in a single DCS system can cause small biases in the retrieved concentrations, but these should be well below 0.1 % in this configuration (Truong et al. 2017, in prep). All these instrument-specific uncertainties are summarized in Table 2.

3.3 DCS precision

Figure 8 shows the precision versus averaging time (determined using the modified Allan deviation) based on the scatter across a 6-hour period over which the CO_2 and CH_4 concentrations are reasonably flat, shown as the highlighted part of Figure 5. (The Allan deviation for H_2O is not calculated because the atmospheric H_2O concentration varies significantly over this time period.) Under perfectly stable concentrations and white instrument noise, the precision should decrease as the square root of averaging time, indicated as a grey line in Figure 8. Initially, the Allan deviations do follow this slope, but the atmospheric concentrations, especially of CO_2, vary over this 6-hour period and the Allan deviations reach a floor at ~ 1000 s. As in (Chen et al., 2016) it is also useful to plot the Allan deviation of the difference in retrieved concentration between the instruments, e.g. ΔXCO_2 and ΔXCH_4 of Figure 6. This removes the atmospheric variability from the Allan deviation and provides information on the relative stability of the two instruments. As it includes contributions from both DCS instruments, it lies above both individual Allan deviations but similarly reaches a floor at ~1000 s, indicating the floor of the individual Allan deviations is likely dominated by instrument rather than atmospheric variability for these data. We note a similar floor is found in (Truong et al., 2016) for static laboratory cell data where it was attributed to the existence of an etalon.

The precision at ~~30-second~~30s and 5- minute averaging time is given at the bottom of Table 1. DCS A has superior CO_2 precision because it has higher received optical comb power in that spectral region, whereas the DCS instruments have similar received power in the CH_4 spectral region and therefore similar CH_4 precisions. Regardless, the precision of either instrument is sufficiently high to measure the characteristic atmospheric fluctuations of these gases on tens-of-seconds timescales.

3.4 Comparison of open-path DCS to a cavity ringdown point sensor (CRDS)

A commercial cavity-ringdown point sensor, Picarro Model 1301[2] (Crosson, 2008), was also located along the path as shown in Figure 2. Its inlet was ~~30 m~~30m above ground on a radio tower, approximately 160 m perpendicular to the DCS beam path. Figure 9 compares the DCS A and CRDS (smoothed to ~~32 s~~32s resolution) time series. In general, their overall shapes agree well with both systems tracking ~40 ppm variations in XCO_2, 200 ppb variations in XCH_4, and 1 % variations in H_2O over days. Nevertheless, there are clear discrepancies in terms of both short-duration spikes and a long-term overall offset between the DCS and CRDS time series.

The short-duration spikes are present in the CRDS time series and presumably arise from the very different spatial sampling of the two instruments. The DCS system measures the integrated column over one kilometer (one way), while the CRDS is a point sensor and therefore much more sensitive to local sources. For example, a 1 m^3 volume of air containing 500 ppm of CO_2 from a vehicle driving under the sampling line will result in a sharp spike in the CRDS data as the air mass passes the sampling inlet. However, that same air mass will result in only a 0.025 % or 0.1 ppm increase in the DCS path-averaged concentration (assuming a 400 ppm background). These spikes in the CRDS time series are damped here by the ~~32-second~~32s smoothing but are occasionally evident especially during the second week. The general scarcity of such events does suggest that the air over the open path is usually fairly well mixed.

The long-term overall offset between the CRDS and DCS data is a consequence of their very different calibrations. The CRDS is tied to the WMO scale for CO_2 and CH_4 by directly injecting known dry WMO-calibrated CO_2/CH_4 mixtures at different trace gas concentrations and different water vapor concentrations into its temperature- and pressure-controlled sampling cavity. This instrument was calibrated shortly after the measurement campaign and should thus have an absolute uncertainty close to that of the WMO-scale uncertainties of ~ 0.07 ppm for CO_2 (Zhao and Tans, 2006) and ~1.5 ppb for CH_4 (Dlugokencky et al., 2005).

[2] The use of trade names is necessary to specify the experimental results and does not imply endorsement by the National Institute of Standards and Technology.

In contrast, the DCS has no instrument-specific calibration but relies completely on a fit to a spectral database to extract the gas concentrations from the measured absorbance across a wide range of ambient pressures and temperatures. Here, we use HITRAN 2008 which has $^{12}CO_2$ linestrength uncertainties of 1-2 %, $^{12}CH_4$ linestrength uncertainties of 10-20 %, and $H_2{}^{16}O$ linestrength uncertainties of 5-10 % (Rothman et al., 2009), leading to a poorer absolute calibration than the WMO-calibrated point sensor. From the data in Figure 9, the differences between the CRDS and DCS data across the two-week period are -3.4 ± 3.4 ppm CO_2, 17 ± 15 ppb CH_4, and 580 ± 462 ppm H_2O at 5-minute averaging. These correspond to relative offsets of -0.85 % for CO_2, 0.94 % for CH_4, and 6.9 % for H_2O, well within the stated uncertainties of HITRAN 2008. In previous DCS measurements, we found slightly different offsets, specifically 1.78 % for CO_2, 0.20 % for CH_4, and 1.74 % for H_2O in (Rieker et al., 2014) and ~1 % for CO_2 in ~~(Giorgetta et al., 2015)~~(Giorgetta et al., 2015). However, these previous data covered much shorter timespans, used an older CRDS point sensor calibration, and may have included small systematic offsets in the DCS systems due to technical issues discussed in Section 3.2.

This basic discrepancy between retrievals based on lineshape parameters from a spectral database and manometric calibrations (WMO standard) is not unique to DCS. Several studies have calibrated the Total Carbon Column Observing Network (TCCON) retrievals against WMO-based instruments (Wunch et al., 2010; Messerschmidt et al., 2011; Geibel et al., 2012; Tanaka et al., 2012). Although TCCON is not a solely HITRAN-based analysis (Wunch et al., 2011), a correction factor of 0.9898 for CO_2, 0.9765 for CH_4, and 1.0183 for H_2O (Wunch et al., 2010) is needed to bring the overall TCCON retrievals into agreement with the WMO-based data. Additionally, theoretical calculations by (Zak et al., 2016) found an approximately 0.5 % difference between CO_2 line parameters from HITRAN 2012 and their density functional theory calculations and an additional 0.5 % difference between the calculations and new measurements by (Devi et al., 2016) in the 1.6-micron region. Certainly this discrepancy between retrievals from HITRAN and WMO-calibrated instruments is not fundamental and further experimental work should lead to improved spectral database parameters and much better agreement. As noted in earlier work on CO_2, it will be important to establish both the correct linestrengths as well as account for complex lineshapes and line mixing (e.g. Devi et al., 2007; Thompson et al., 2012; Bui et al., 2014; Long et al., 2015; Devi et al., 2016). A direct comparison of the open-path DCS spectra acquired here and laboratory DCS spectra acquired for WMO-calibrated gas samples can contribute to these future improvements and is planned. Finally, we emphasize that because the DCS instruments record the atmospheric absorption without instrument distortions, as spectral models improve, past open-path spectra can be refit with reduced uncertainty.

An accurate path-averaged air temperature is also important to avoid systematic offsets. Unlike vertical total-column measurements through the entire atmosphere, km-scale open horizontal paths should have relatively low temperature inhomogeneities of around a few degrees C, and thus the use of a single “path averaged” temperature in the fit is sufficient for accurate retrievals. We verified this through a sensitivity study comparing retrievals for simulated spectra with temperature gradients up to 10 °C over the path; the resulting bias was below 0.03 ppm CO_2 (0.007 %) and 0.4 ppb CH_4 (0.022 %), as shown in Table 2. On the other hand, any error in the path-averaged temperature can bias the mole fractions through two effects. First, the retrieved path-averaged concentration will vary weakly with temperature because of temperature-dependent line parameters. Second and dominantly, the final mole fraction calculation requires normalization by the air density. Here, this density is calculated from the ideal gas law using the measured air pressure and path-averaged temperature. Therefore, a fractional error in temperature leads to a corresponding fractional error in mole fraction. For example, a 0.15 % uncertainty in mole fraction requires 0.5 °C uncertainty in the path-averaged air temperature. (See Table 2.) We verified that this simple linear relationship is valid up to a temperature uncertainty of 10 °C in a sensitivity study. From the discussion in Appendix A, the use of a point temperature sensor near the end of the open path is clearly insufficient to achieve <0.5 °C uncertainty at many times of the

day. Instead, for the data here, we have used the fitted path-averaged temperature, as discussed in Section 2.~~4~~5. The approach effectively relies on the spectral database but, in this case, on the variation in the Boltzmann distribution of the J-level population with temperature. In Table 2, we have taken a hopefully conservative uncertainty of 0.5 °C for the path-averaged temperature, but more work is needed to establish the true uncertainty from these retrieved values. ~~Finally, we~~We note the fractional uncertainty in the measured atmospheric pressure from the sensor or altitude-based pressure changes across the optical path was below 0.36 %.

Finally, the calculation of the dry mole fraction requires an accurate removal of the water concentration. We do retrieve the water concentration with a high precision from the fits. As shown in Table 2, the dominant uncertainty in the water concentration is again the line strengths from the spectral database.

4. Diurnal cycles and source analysis

The two weeks of open path data are analyzed for diurnal cycles, as shown in Figure 10 with the intent of an initial understanding of CO_2 and CH_4 sources. For this analysis, the wind speed and wind direction were taken from the NCAR Mesa weather data (ftp://ftp.eol.ucar.edu/pub/archive/weather/mesa/), while the gas concentrations are from DCS A.

4.1 Carbon dioxide

As expected, the median of the diurnal cycle for CO_2 shows a peak in the early to mid-morning from commuter traffic after which the CO_2 concentration decreases as the boundary layer rises. It remains approximately steady throughout the afternoon, decreases to a minimum between 19:00 and 20:00, and then increases slightly overnight as the boundary layer collapses. We hypothesize that the afternoon behavior is due to the change in wind direction. Often overnight and through early morning the wind blows from the west to southwest, which brings in cleaner background air from the mountains bordering Boulder. However, in late morning the predominant wind direction shifts to the east and southeast, possibly bringing in higher CO_2 concentrations from the Denver metropolitan area – which lies approximately 30 km to the southeast of Boulder – over the course of the afternoon. Typically, the evening wind shifts back to out of the west, once again bringing in the cleaner mountain air and with it a decrease in CO_2 concentration.

4.2 Methane

Methane has a significantly weaker diurnal cycle than carbon dioxide, which is consistent with a species that lacks significant diurnally-varying local sources. Rather, its concentration follows expected variations in the boundary layer height; the concentration increases overnight into the early morning as the boundary layer collapses, and then decreases during the late morning through afternoon as the boundary layer rises again. The largest likely methane source near Boulder is local oil/gas fields, but these typically lie to the northeast, while the wind directions are generally out of the west to southeast. It is also possible that the methane comes from leaking natural gas infrastructure within the city.

5 Conclusions

Here we provide the first quantitative comparison of open-path dual comb spectroscopy instruments. The dual-comb spectrometers were based on fully phase-coherent and stabilized fiber frequency combs and operated nearly continuously over a two-week period. We performed these measurements over adjacent ~~2-kilometer~~2km round-trip paths to measure concentrations of dry CO_2, dry CH_4, H_2O, and HDO. The measured atmospheric absorbance spectra agree to better than 10^{-3}. Correspondingly, we find excellent agreement between the retrieved concentrations from the two instruments without the need for instrument calibration: over two weeks of near-continuous

measurements, the retrieved CO_2 concentrations agree to better than 0.14 % (0.57 ppm), CH_4 concentrations agrees to better than 0.35 % (7.0 ppb), and H_2O concentrations agrees to better than 0.4 % (36 ppm). These values are very close to the WMO compatibility ~~goals~~standards. The remaining disagreement is likely due to scattered stray light, polarization dependencies, and residual comb phase noise. We further compare the DCS measurements to a cavity ringdown point sensor located along our path. The measured dry CO_2 mole fraction agrees to within 1 %, the CH_4 dry mole fraction to within 1.2 %, and H_2O mole fraction to within 6.2 %. However, this CRDS point sensor is directly calibrated to the WMO scale for CO_2 and CH_4 while the DCS results are based on HITRAN 2008; we attribute the disagreement in CO_2 and CH_4 to inaccurate line parameters in the HITRAN database. (Most of the water discrepancy is attributed to the imperfect absolute water calibration of the CRDS point sensor.) Further improvements to the spectral database should reduce these discrepancies. Finally, this open-path DCS can exploit even broader spectrum combs up to 2.3 µm and down to 1.1 µm (Zolot et al., 2012; Okubo et al., 2015), which would enable measurements of similar quality for $^{13}CO_2$, NH_3, N_2O, and O_2. These results make open-path DCS a promising new system for greenhouse gas flux measurements from distributed sources.

The authors declare that they have no conflict of interest.

Acknowledgements: We thank T. Newburger and K. McKain for assistance with the CRDS calibrations, T. Bullet and J. Kofler for assistance in setting up the CRDS sampling, and R. Thalman for detailed long-path instrument correlation data, and A.J. Fleischer and A. Karion for assistance with the manuscript. This work was funded by the Defense Advanced Research Program Agency DSO SCOUT program, ARPA-E MONITOR program under Award Number DE-AR0000539, and J. Whetstone and the NIST Greenhouse Gas and Climate Science Initiative. EMW and KCC are supported by National Research Council postdoctoral fellowships.

References

Bui, T. Q., Long, D. A., Cygan, A., Sironneau, V. T., Hogan, D. W., Rupasinghe, P. M., Ciuryło, R., Lisak, D. and Okumura, M.: Observations of Dicke narrowing and speed dependence in air-broadened CO_2 lineshapes near 2.06 µm, J. Chem. Phys., 141(17), 174301, doi:10.1063/1.4900502, 2014.

Chen, J., Viatte, C., Hedelius, J. K., Jones, T., Franklin, J. E., Parker, H., Gottlieb, E. W., Wennberg, P. O., Dubey, M. K. and Wofsy, S. C.: Differential column measurements using compact solar-tracking spectrometers, Atmos Chem Phys, 16(13), 8479–8498, doi:10.5194/acp-16-8479-2016, 2016.

Ciais, P., Rayner, P., Chevallier, F., Bousquet, P., Logan, M., Peylin, P. and Ramonet, M.: Atmospheric inversions for estimating CO_2 fluxes: methods and perspectives, Clim. Change, 103(1–2), 69–92, doi:10.1007/s10584-010-9909-3, 2010.

Coddington, I., Swann, W. C. and Newbury, N. R.: Coherent multiheterodyne spectroscopy using stabilized optical frequency combs, Phys. Rev. Lett., 100(1), 013902, doi:10.1103/PhysRevLett.100.013902, 2008.

Coddington, I., Newbury, N. and Swann, W.: Dual-comb spectroscopy, Optica, 3(4), 414–426, doi:10.1364/OPTICA.3.000414, 2016.

Conde, V., Robidoux, P., Avard, G., Galle, B., Aiuppa, A., Muñoz, A. and Giudice, G.: Measurements of volcanic SO_2 and CO_2 fluxes by combined DOAS, Multi-GAS and FTIR observations: a case study from Turrialba and Telica volcanoes, Int. J. Earth Sci., 103(8), 2335–2347, doi:10.1007/s00531-014-1040-7, 2014.

Cossel, K. C., Waxman, E. M., Giorgetta, F. R., Cermak, M., Coddington, I. R., Hesselius, D., Ruben, S., Swann, W. C., Truong, G.-W., Rieker, G. B. and Newbury, N. R.: Open-path dual-comb spectroscopy to an airborne retroreflector, Optica, 4(7), 724–728, doi:10.1364/OPTICA.4.000724, 2017.

Crosson, E. R.: A cavity ring-down analyzer for measuring atmospheric levels of methane, carbon dioxide, and water vapor, Appl. Phys. B, 92(3), 403–408, doi:10.1007/s00340-008-3135-y, 2008.

Cundiff, S. T. and Ye, J.: Colloquium: Femtosecond optical frequency combs, Rev Mod Phys, 75(1), 325–342, doi:10.1103/RevModPhys.75.325, 2003.

Devi, V. M., Benner, D. C., Brown, L. R., Miller, C. E. and Toth, R. A.: Line mixing and speed dependence in CO_2 at 6227.9 cm^{-1}: Constrained multispectrum analysis of intensities and line shapes in the 30013 ← 00001 band, J. Mol. Spectrosc., 245(1), 52–80, doi:10.1016/j.jms.2007.05.015, 2007.

Devi, V. M., Benner, D. C., Sung, K., Brown, L. R., Crawford, T. J., Miller, C. E., Drouin, B. J., Payne, V. H., Yu, S., Smith, M. A. H., Mantz, A. W. and Gamache, R. R.: Line parameters including temperature dependences of self- and air-broadened line shapes of 12C16O2: 1.6-μm region, J. Quant. Spectrosc. Radiat. Transf., 177, 117–144, doi:10.1016/j.jqsrt.2015.12.020, 2016.

Dlugokencky, E. J., Myers, R. C., Lang, P. M., Masarie, K. A., Crotwell, A. M., Thoning, K. W., Hall, B. D., Elkins, J. W. and Steele, L. P.: Conversion of NOAA atmospheric dry air CH_4 mole fractions to a gravimetrically prepared standard scale, J. Geophys. Res. Atmospheres, 110(D18), D18306, doi:10.1029/2005JD006035, 2005.

EPA: EPA Handbook: Optical Remote Sensing for Measurement and Monitoring of Emissions, [online] Available from: https://www3.epa.gov/ttn/emc/guidlnd/gd-052.pdf (Accessed 2 March 2017), n.d.

Fante, R. L.: Electromagnetic beam propagation in turbulent media, Proc. IEEE, 63(12), 1669–1692, doi:10.1109/PROC.1975.10035, 1975.

Frey, M., Hase, F., Blumenstock, T., Groß, J., Kiel, M., Mengistu Tsidu, G., Schäfer, K., Sha, M. K. and Orphal, J.: Calibration and instrumental line shape characterization of a set of portable FTIR spectrometers for detecting greenhouse gas emissions, Atmos Meas Tech, 8(7), 3047–3057, doi:10.5194/amt-8-3047-2015, 2015.

Geibel, M. C., Messerschmidt, J., Gerbig, C., Blumenstock, T., Chen, H., Hase, F., Kolle, O., Lavrič, J. V., Notholt, J., Palm, M., Rettinger, M., Schmidt, M., Sussmann, R., Warneke, T. and Feist, D. G.: Calibration of column-averaged CH_4 over European TCCON FTS sites with airborne in-situ measurements, Atmos Chem Phys, 12(18), 8763–8775, doi:10.5194/acp-12-8763-2012, 2012.

Giorgetta, F. R., Rieker, G. B., Baumann, E., Swann, W. C., Sinclair, L. C., Kofler, J., Coddington, I. and Newbury, N. R.: Broadband Phase Spectroscopy over Turbulent Air Paths, Phys. Rev. Lett., 115(10), 103901, doi:10.1103/PhysRevLett.115.103901, 2015.

Hak, C., Pundt, I., Trick, S., Kern, C., Platt, U., Dommen, J., Ordóñez, C., Prévôt, A. S. H., Junkermann, W., Astorga-Lloréns, C. and others: Intercomparison of four different in-situ techniques for ambient formaldehyde measurements in urban air, Atmospheric Chem. Phys., 5(11), 2881–2900, 2005.

Hall, J. L.: Nobel Lecture: Defining and measuring optical frequencies, Rev. Mod. Phys., 78(4), 1279–1295, 2006.

Hänsch, T. W.: Nobel Lecture: Passion for precision, Rev. Mod. Phys., 78(4), 1297–1309, doi:10.1103/RevModPhys.78.1297, 2006.

Hedelius, J. K., Viatte, C., Wunch, D., Roehl, C. M., Toon, G. C., Chen, J., Jones, T., Wofsy, S. C., Franklin, J. E., Parker, H., Dubey, M. K. and Wennberg, P. O.: Assessment of errors and biases in retrievals of XCO_2, XCH_4, XCO, and XN_2O from a 0.5 cm^{-1} resolution solar-viewing spectrometer, Atmos Meas Tech, 9(8), 3527–3546, doi:10.5194/amt-9-3527-2016, 2016.

Ideguchi, T.: Dual-Comb Spectroscopy, Opt. Photonics News, 28, 32–39, 2017.

Lauvaux, T. and Davis, K. J.: Planetary boundary layer errors in mesoscale inversions of column-integrated CO_2 measurements, J. Geophys. Res. Atmospheres, 119(2), 490–508, doi:10.1002/2013JD020175, 2014.

Lauvaux, T., Uliasz, M., Sarrat, C., Chevallier, F., Bousquet, P., Lac, C., Davis, K. J., Ciais, P., Denning, A. S. and Rayner, P. J.: Mesoscale inversion: first results from the CERES campaign with synthetic data, Atmos Chem Phys, 8(13), 3459–3471, doi:10.5194/acp-8-3459-2008, 2008.

Lauvaux, T., Schuh, A. E., Bocquet, M., Wu, L., Richardson, S., Miles, N. and Davis, K. J.: Network design for mesoscale inversions of CO_2 sources and sinks, Tellus B, 64(0), doi:10.3402/tellusb.v64i0.17980, 2012.

Long, D. A., Wójtewicz, S., Miller, C. E. and Hodges, J. T.: Frequency-agile, rapid scanning cavity ring-down spectroscopy (FARS-CRDS) measurements of the (30012)←(00001) near-infrared carbon dioxide band, J. Quant. Spectrosc. Radiat. Transf., 161, 35–40, doi:10.1016/j.jqsrt.2015.03.031, 2015.

Messerschmidt, J., Geibel, M. C., Blumenstock, T., Chen, H., Deutscher, N. M., Engel, A., Feist, D. G., Gerbig, C., Gisi, M., Hase, F., Katrynski, K., Kolle, O., Lavrič, J. V., Notholt, J., Palm, M., Ramonet, M., Rettinger, M., Schmidt, M., Sussmann, R., Toon, G. C., Truong, F., Warneke, T., Wennberg, P. O., Wunch, D. and Xueref-Remy, I.: Calibration of TCCON column-averaged CO_2: the first aircraft campaign over European TCCON sites, Atmos Chem Phys, 11(21), 10765–10777, doi:10.5194/acp-11-10765-2011, 2011.

Okubo, S., Iwakuni, K., Inaba, H., Hosaka, K., Onae, A., Sasada, H. and Hong, F.-L.: Ultra-broadband dual-comb spectroscopy across 1.0–1.9 μm, Appl. Phys. Express, 8(8), 082402, doi:10.7567/APEX.8.082402, 2015.

Reiche, N., Westerkamp, T., Lau, S., Borsdorf, H., Dietrich, P. and Schütze, C.: Comparative study to evaluate three ground-based optical remote sensing techniques under field conditions by a gas tracer experiment, Environ. Earth Sci., 72(5), 1435–1441, doi:10.1007/s12665-014-3312-8, 2014.

Rieker, G. B., Giorgetta, F. R., Swann, W. C., Kofler, J., Zolot, A. M., Sinclair, L. C., Baumann, E., Cromer, C., Petron, G., Sweeney, C., Tans, P. P., Coddington, I. and Newbury, N. R.: Frequency-comb-based

remote sensing of greenhouse gases over kilometer air paths, Optica, 1(5), 290–298, doi:10.1364/OPTICA.1.000290, 2014.

Rothman, L. S., Gordon, I. E., Barbe, A., Benner, D. C., Bernath, P. E., Birk, M., Boudon, V., Brown, L. R., Campargue, A., Champion, J. P., Chance, K., Coudert, L. H., Dana, V., Devi, V. M., Fally, S., Flaud, J. M., Gamache, R. R., Goldman, A., Jacquemart, D., Kleiner, I., Lacome, N., Lafferty, W. J., Mandin, J. Y., Massie, S. T., Mikhailenko, S. N., Miller, C. E., Moazzen-Ahmadi, N., Naumenko, O. V., Nikitin, A. V., Orphal, J., Perevalov, V. I., Perrin, A., Predoi-Cross, A., Rinsland, C. P., Rotger, M., Simeckova, M., Smith, M. A. H., Sung, K., Tashkun, S. A., Tennyson, J., Toth, R. A., Vandaele, A. C. and Vander Auwera, J.: The HITRAN 2008 molecular spectroscopic database, J. Quant. Spectrosc. Radiat. Transf., 110(9–10), 533–572, doi:10.1016/j.jqsrt.2009.02.013, 2009.

Schiller, S.: Spectrometry with frequency combs, Opt Lett, 27(9), 766–768, 2002.

Schliesser, A., Brehm, M., Keilmann, F. and van der Weide, D.: Frequency-comb infrared spectrometer for rapid, remote chemical sensing, Opt. Express, 13(22), 9029–9038, doi:10.1364/OPEX.13.009029, 2005.

Shao, L., Wang, W., Griffiths, P. R. and Leytem, A. B.: Increasing the Quantitative Credibility of Open-Path Fourier Transform Infrared (FT-IR) Spectroscopic Data, with Focus on Several Properties of the Background Spectrum, Appl. Spectrosc., 67(3), 335–341, doi:10.1366/12-06901, 2013.

Sinclair, L. C., Deschênes, J.-D., Sonderhouse, L., Swann, W. C., Khader, I. H., Baumann, E., Newbury, N. R. and Coddington, I.: Invited Article: A compact optically coherent fiber frequency comb, Rev. Sci. Instrum., 86(8), 081301, doi:10.1063/1.4928163, 2015.

Smith, T. E. L., Wooster, M. J., Tattaris, M. and Griffith, D. W. T.: Absolute accuracy and sensitivity analysis of OP-FTIR retrievals of CO_2, CH_4 and CO over concentrations representative of “clean air” and “polluted plumes,” Atmos Meas Tech, 4(1), 97–116, doi:10.5194/amt-4-97-2011, 2011.

Tanaka, T., Miyamoto, Y., Morino, I., Machida, T., Nagahama, T., Sawa, Y., Matsueda, H., Wunch, D., Kawakami, S. and Uchino, O.: Aircraft measurements of carbon dioxide and methane for the calibration of ground-based high-resolution Fourier Transform Spectrometers and a comparison to GOSAT data measured over Tsukuba and Moshiri, Atmos Meas Tech, 5(8), 2003–2012, doi:10.5194/amt-5-2003-2012, 2012.

Tans, P. and Zellweger, C.: 18th WMO/IAEA Meeting on Carbon Dioxide, Other Greenhouse Gases and Related Tracers Measurement Techniques, GAW, La Jolla, CA, USA. [online] Available from: http://www.wmo.int/pages/prog/arep/gaw/documents/FINAL_GAW_REPORT_229.pdf (Accessed 8 February 2017), 2015.

Thalman, R., Baeza-Romero, M. T., Ball, S. M., Borrás, E., Daniels, M. J. S., Goodall, I. C. A., Henry, S. B., Karl, T., Keutsch, F. N., Kim, S., Mak, J., Monks, P. S., Muñoz, A., Orlando, J., Peppe, S., Rickard, A. R., Ródenas, M., Sánchez, P., Seco, R., Su, L., Tyndall, G., Vázquez, M., Vera, T., Waxman, E. and Volkamer, R.: Instrument intercomparison of glyoxal, methyl glyoxal and NO_2 under simulated atmospheric conditions, Atmos Meas Tech, 8(4), 1835–1862, doi:10.5194/amt-8-1835-2015, 2015.

Thoma, E. D., Shores, R. C., Thompson, E. L., Harris, D. B., Thorneloe, S. A., Varma, R. M., Hashmonay, R. A., Modrak, M. T., Natschke, D. F. and Gamble, H. A.: Open-Path Tunable Diode Laser Absorption

Spectroscopy for Acquisition of Fugitive Emission Flux Data, J. Air Waste Manag. Assoc., 55(5), 658–668, doi:10.1080/10473289.2005.10464654, 2005.

Thompson, D. R., Chris Benner, D., Brown, L. R., Crisp, D., Malathy Devi, V., Jiang, Y., Natraj, V., Oyafuso, F., Sung, K., Wunch, D., Castaño, R. and Miller, C. E.: Atmospheric validation of high accuracy CO_2 absorption coefficients for the OCO-2 mission, J. Quant. Spectrosc. Radiat. Transf., 113(17), 2265–2276, doi:10.1016/j.jqsrt.2012.05.021, 2012.

Truong, G.-W., Waxman, E. M., Cossel, K. C., Baumann, E., Klose, A., Giorgetta, F. R., Swann, W. C., Newbury, N. R. and Coddington, I.: Accurate frequency referencing for fieldable dual-comb spectroscopy, Opt. Express, 24(26), 30495, doi:10.1364/OE.24.030495, 2016.

Truong, G.-W., Giorgetta, F. R., Cossel, K.C., Waxman, E. M., Newbury, N. R., and Coddington, I.: Effects of Phase Noise on Coherent Dual-Comb Spectroscopy, in preparation, to be submitted to Optics Letters, 2017.

Wunch, D., Toon, G. C., Wennberg, P. O., Wofsy, S. C., Stephens, B. B., Fischer, M. L., Uchino, O., Abshire, J. B., Bernath, P., Biraud, S. C., Blavier, J.-F. L., Boone, C., Bowman, K. P., Browell, E. V., Campos, T., Connor, B. J., Daube, B. C., Deutscher, N. M., Diao, M., Elkins, J. W., Gerbig, C., Gottlieb, E., Griffith, D. W. T., Hurst, D. F., Jiménez, R., Keppel-Aleks, G., Kort, E. A., Macatangay, R., Machida, T., Matsueda, H., Moore, F., Morino, I., Park, S., Robinson, J., Roehl, C. M., Sawa, Y., Sherlock, V., Sweeney, C., Tanaka, T. and Zondlo, M. A.: Calibration of the Total Carbon Column Observing Network using aircraft profile data, Atmos Meas Tech, 3(5), 1351–1362, doi:10.5194/amt-3-1351-2010, 2010.

Wunch, D., Toon, G. C., Blavier, J.-F. L., Washenfelder, R. A., Notholt, J., Connor, B. J., Griffith, D. W. T., Sherlock, V. and Wennberg, P. O.: The Total Carbon Column Observing Network, Philos. Trans. R. Soc. Math. Phys. Eng. Sci., 369(1943), 2087–2112, doi:10.1098/rsta.2010.0240, 2011.

Zak, E., Tennyson, J., Polyansky, O. L., Lodi, L., Zobov, N. F., Tashkun, S. A. and Perevalov, V. I.: A room temperature CO_2 line list with ab initio computed intensities, J. Quant. Spectrosc. Radiat. Transf., 177, 31–42, doi:10.1016/j.jqsrt.2015.12.022, 2016.

Zhao, C. L. and Tans, P. P.: Estimating uncertainty of the WMO mole fraction scale for carbon dioxide in air, J. Geophys. Res. Atmospheres, 111(D8), D08S09, doi:10.1029/2005JD006003, 2006.

Zolot, A. M., Giorgetta, F. R., Baumann, E., Nicholson, J. W., Swann, W. C., Coddington, I. and Newbury, N. R.: Direct-comb molecular spectroscopy with accurate, resolved comb teeth over 43 THz, Opt. Lett., 37(4), 638–640, doi:10.1364/OL.37.000638, 2012.

Zolot, A. M., Giorgetta, F. R., Baumann, E., Swann, W. C., Coddington, I. and Newbury, N. R.: Broad-band frequency references in the near-infrared: Accurate dual comb spectroscopy of methane and acetylene, J. Quant. Spectrosc. Radiat. Transf., 118, 26–39, doi:10.1016/j.jqsrt.2012.11.024, 2013.

	DCS A	DCS B
Design Details		
Comb 1 repetition rate (f_r)	~200 MHz	~204 MHz
Difference in repetition rate (Δf_r)	624 Hz	870 Hz
Spectral filtering	Before combining combs	After combining combs
Booster amplifier	Yes	No
Average power launched	4 mW	1.5 mW
Filtered spectral output	6376 to 6023 cm^{-1}	6359 to 6003 cm^{-1}
Telescope design	Home-built 3”-diameter off-axis telescope	Modified commercial 6”-diameter Ritchey-Chretien telescope
Retroreflector	2.5” HCC, 5 arc seconds	5” HCC, 5 arc seconds
Round-trip path length	1950.17 m	1963.67 m
Typical averaging time	32 s	28 s
Performance Metrics		
30-second precision	0.90 ppm ~~CO_2~~XCO_2, 9.6 ppb ~~CH_4~~XCH_4	2.15 ppm ~~CO_2~~XCO_2, 11.5 ppb ~~CH_4~~XCH_4
5-minute precision	0.24 ppm ~~CO_2~~XCO_2, 2.1 ppb ~~CH_4~~XCH_4	0.60 ppm ~~CO_2~~XCO_2, 3.2 ppb ~~CH_4~~XCH_4

Table 1: Specifications of the two DCS systems. HCC: hollow corner cube

Systematic source [effect]	Effect on retrieved ~~CO_2~~XCO_2	Effect on retrieved ~~CH_4~~XCH_4	Effect on retrieved H_2O
Fitting procedure [initial guess, baseline polynomial order and window size]	0.07 ppm	1.4 ppb	4 ppm
Rf detection and processing [rf reflections, ADC nonlinearities]	0.16 ppm	0.34 ppb	1.0 ppm
Telescope system [Scattered light, polarization effects]	0.45 ppm	1.5 ppb	56 ppm
Spectral database [linestrengths in HITRAN 2008]	1-2 %	10-20 %	5-10 %
Temperature path inhomogeneities [if <10 °C across path]	0.024 ppm	0.36 ppb	3.52 ppm
Path-averaged temperature [for 0.5 °C uncertainty]	0.64 ppm	2.9 ppb	8.6 ppm
Water correction [~10 % line strength uncertainty]	0.4 ppm	2 ppb	N/A

Table 2: List of systematic uncertainties. See discussion in Section 3.2 and 3.4 for more details. Upper half of table: instrument-specific systematics ~~due to hardware and software.~~. Lower half of the table: model-dependent systematics ~~due to~~common to both instruments. The final row is the estimated added uncertainty from the water correction, which is dominated by the nominal ~ 10% line strength uncertainty of the spectral ~~model and temperature uncertainties.~~database. (The fit uncertainty for the retrieved water concentration is much lower at 0.0065%.)

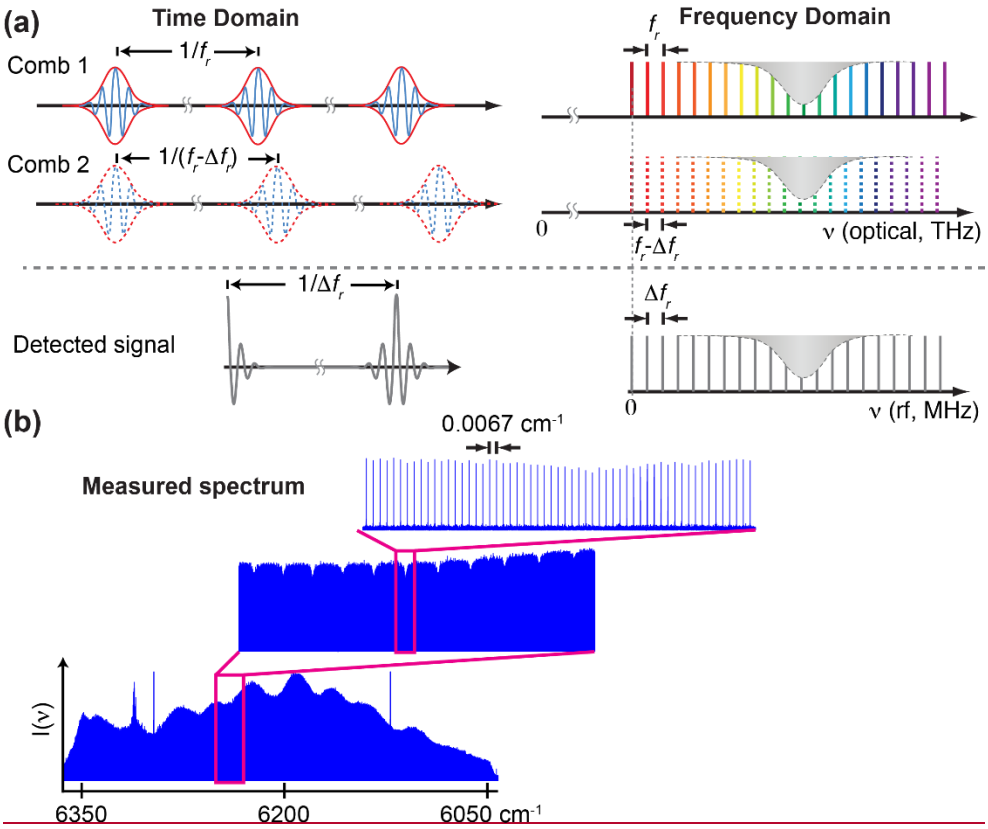
(a)
Time Domain
Frequency Domain
Comb 1
1/f_r
Comb 2
1/(f_r-Δf_r)
f_r
0
ν (optical, THz)
f_r-Δf_r
1/Δf_r
Detected signal
Δf_r
0
ν (rf, MHz)
(b)
0.0067 cm-1
Measured spectrum
I(ν)
6350
6200
6050 cm-1

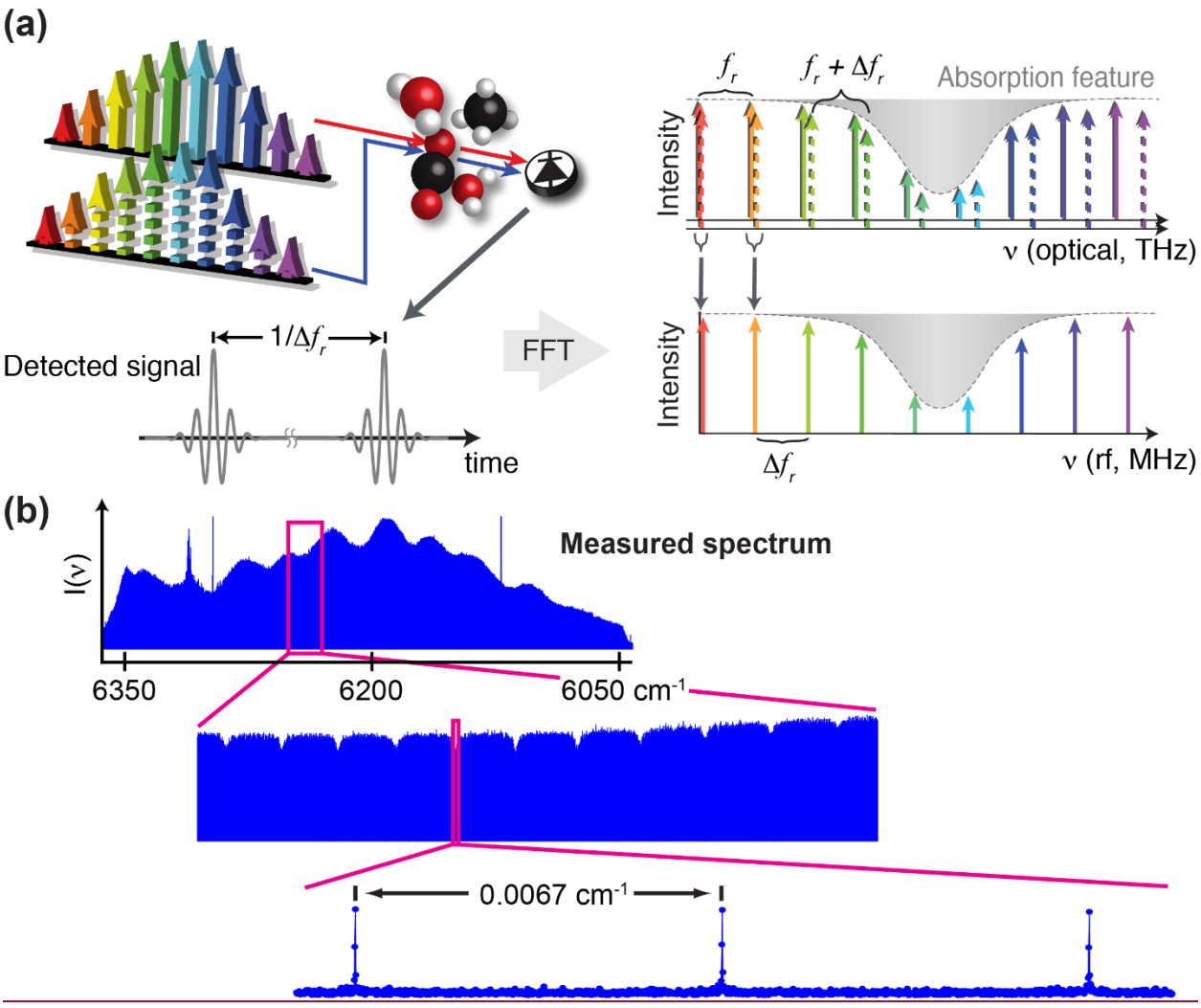

Figure 1. (a) ~~Time and frequency domain overview of~~In dual-~~-~~comb spectroscopy~~. Two~~ two frequency combs (solid and dashed) are phase-locked together with slightly different comb tooth separation (e.g. pulse repetition rates) of f_r and f_r ~~+~~+Δf_r ~~. Their detected heterodyne signal~~ as seen on the right-hand side. The combs pass through a gas sample and are heterodyned on a detector to generate a signal. In the time domain (left hand side), this signal is a series of interferograms ~~in the time domain, or equivalently a comb in the radio frequency (rf) domain. Provided~~, similar to Fourier Transform spectroscopy, whose Fourier transform yields a spectrum. In the ~~combs are sufficiently coherent and Nyquist sampling conditions are met,~~frequency domain (right hand side), each individual pair of comb teeth yields a rf heterodyne signal with an amplitude equal to the product of the comb teeth. Because of the Vernier-like offset in repetition rates, the rf ~~comb tooth maps to a particular, known~~frequency generated by each pair of optical teeth is distinct, giving a one-to-one mapping between rf comb teeth and optical frequency comb teeth. As a result, the x-axis of the measured rf spectrum can simply be scaled to generate the optical spectrum. A more detailed explanation is given in (Coddington et al., 2008)~~. As a result, the optical~~ and references therein. (b) Actual spectrum ~~can be obtained~~ from ~~the magnitude of each rf comb tooth versus the average optical frequency of the relevant comb tooth pair. (b) Actual DCS spectrum acquired~~ DCS A over 1.15 seconds ~~for DCS A~~ after transmission ~~over~~through a 2-km air path. The overall shape is governed by the comb spectrum but there are narrow absorption dips present from atmospheric gases, as shown in the first expanded view. The second expanded view shows the fully resolved rf comb teeth with time-bandwidth limited widths. The highly resolved nature of these spectral elements ~~translates to~~ follows the cartoon in part (a) and reflects the negligible instrument lineshape, set by the narrow comb linewidths. ~~The~~Here, each rf tooth represents an optical sample ~~points are separated by~~ with a separation of 0.0067 cm^{-1} (or f_r =200 MHz). For ~~long-term averaging~~longer acquisition times, we implement coherent co-adding of interferograms that ~~effectively measures the power at the individual rf comb teeth~~maintains this precise optical sampling of the absorbance spectrum (Coddington et al., 2008)

699
700 .

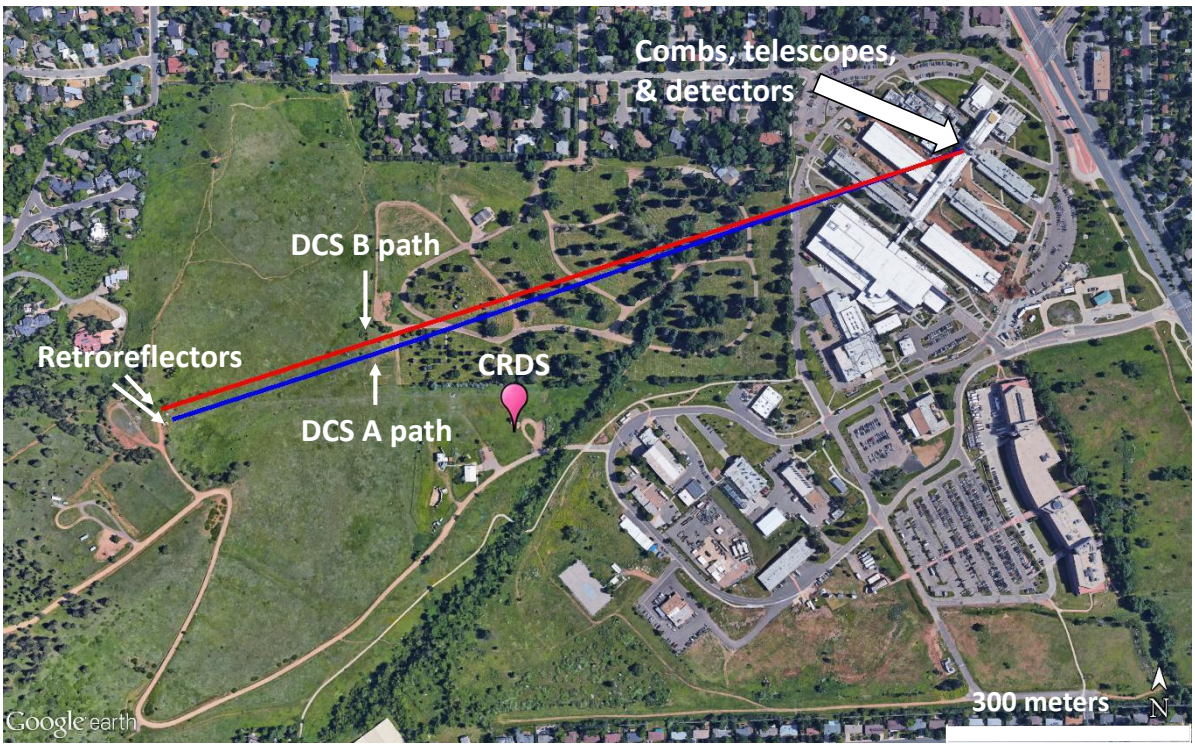

Figure 2. Setup for the open-path dual-comb spectrometer (DCS) comparison at the NIST Boulder CO campus. The main components for DCS A and DCS B are housed in a rooftop laboratory, including the frequency combs, telescope, receiver, and processor. For each DCS, the combined comb light is launched from a telescope, travels ~1 km through the atmosphere to a retroreflector, and returns to the telescope where it is collected, detected and processed. A separate cavity ringdown point sensor (CRDS) is located nearby with an inlet on a 30-m tower that is located ~160 meters from the nearest point of the free-space DCS paths.

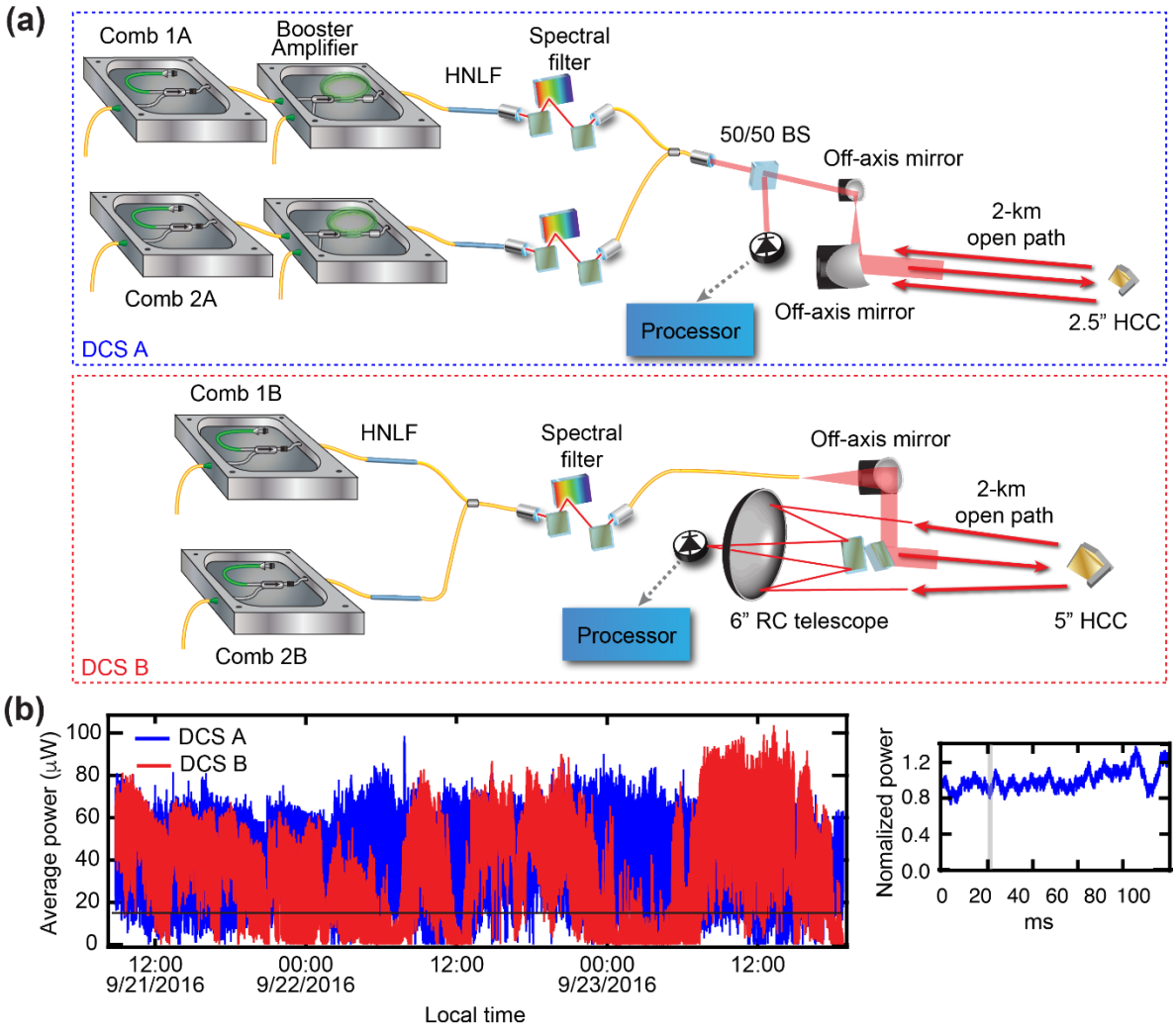

709

710 *Figure 3. (a) Configuration of DCS A and DCS B, both of which are based on fully self-referenced fiber-laser frequency combs. See*
711 *text and Table I for details. DCS A includes a booster amplifier for higher launched optical power than DCS B. (b) Average optical*
712 *return power for DCS A (blue) and DCS B (red) measured at the detector over about 2.5 days. The horizontal black line shows the*
713 *approximate minimum power for useable SNR (15 μW). Inset: The normalized power fluctuations for DCS A over 100 ms. The*
714 *fluctuations are from turbulence and have a characteristic timescale much longer than the acquisition time for a single DCS*
715 *spectrum ~~is~~, shown by the thickness of the vertical grey bar, and therefore do not lead to overall distortions in the spectrum. RC:*
716 *Ritchey-Chretien; HNLF: highly nonlinear fiber; HCC: hollow corner cube retroreflector; BS: beam splitter.*

717

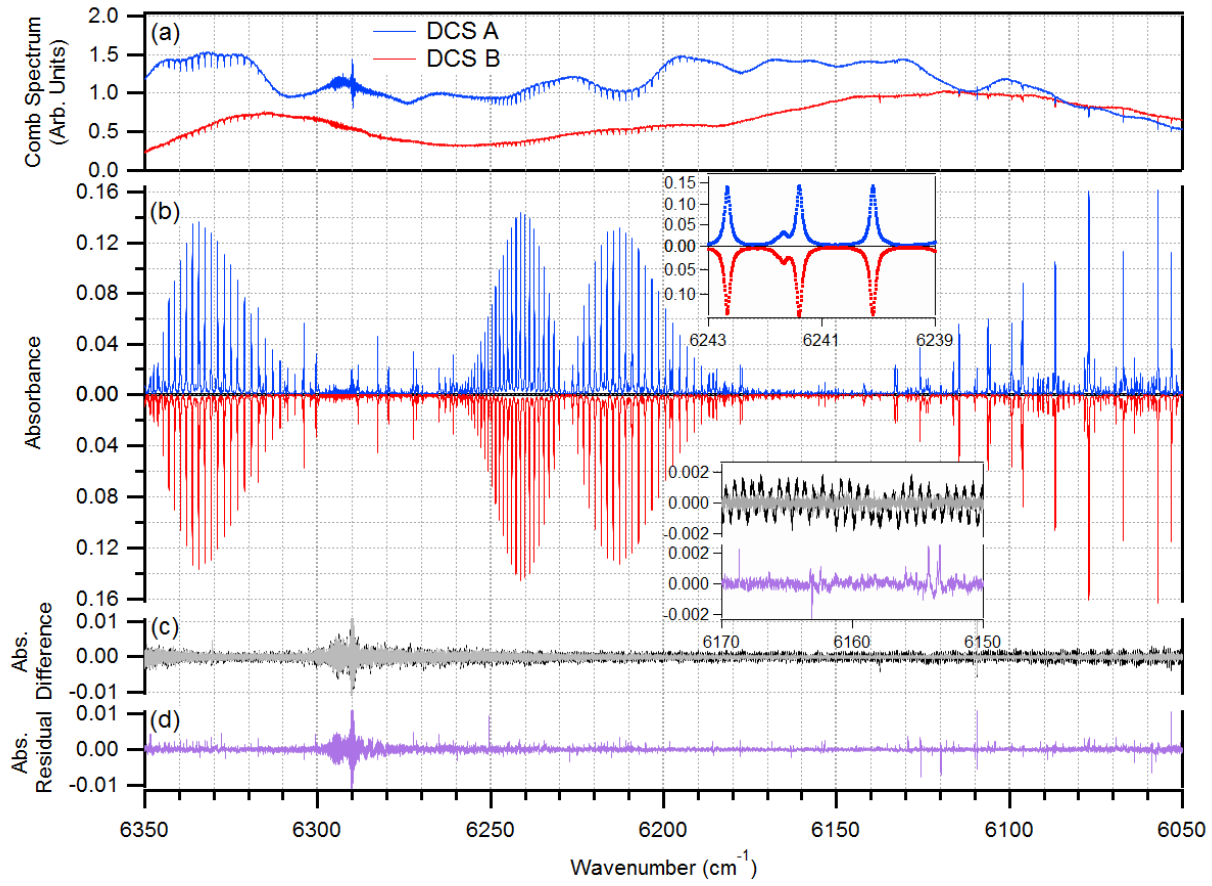

Figure 4. Raw spectra from DCS A (blue) and DCS B (red). (b) Corresponding baseline-corrected absorption spectra averaged for a three-hour period. The spectra overlap completely on this scale so the DCS A absorbance has been flipped about zero. Inset: expanded view of several CO_2 lines. (c) Difference between the absorption spectra from DCS A and DCS B. The difference is shown both before (black trace) and after (grey trace) removing an etalon structure and agree to better than 5×10^{-4} after the etalon is removed. Inset: Expanded view. (d) Residuals from a fit of the DCS A spectrum to HITRAN 2008. In general, the residuals are lower noise than the difference spectrum because of the higher signal-to-noise ratio of the DCS A than DCS B, but there are clear structures present near absorption lines due to imperfect line shapes of the spectral database.

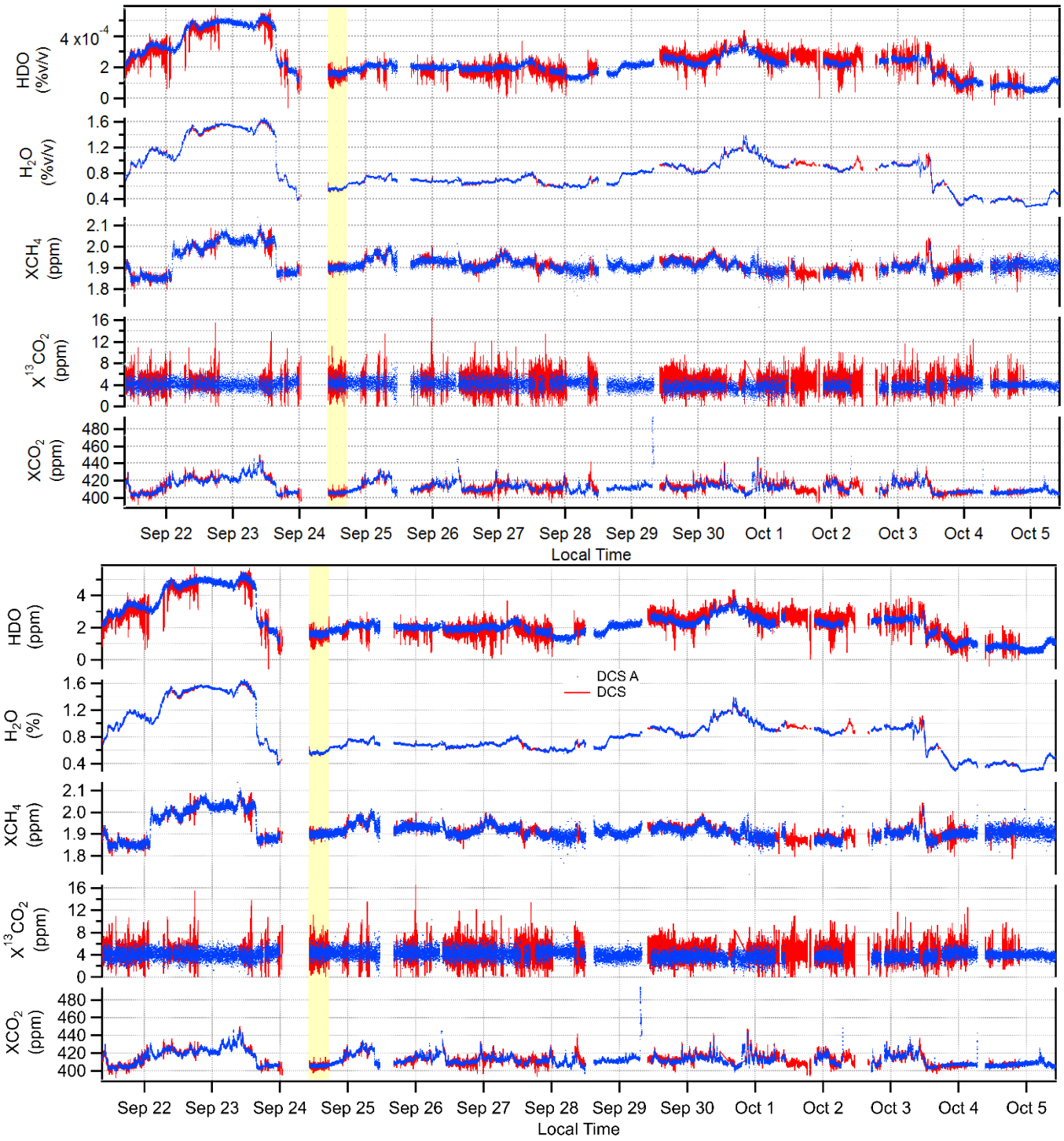

Figure 5. Concentration retrievals from DCS A (blue dots) and DCS B (red lines) for HDO ~~(% by volume)~~(ppm) H_2O ~~(% by volume),~~(%), dry CH_4, dry CO_2 and dry $^{13}CO_2$ over two weeks at 30-second intervals. Excellent agreement is observed between both systems for all species, though it is clear that over this path length $^{13}CO_2$ does not provide a strong enough signal to retrieve reliably. Highlighted section: 6-hour, well-mixed period over which Allan deviations (Figure 8) are calculated. Missing data is primarily due to telescope misalignment and less frequently, phase lock by one of the combs.

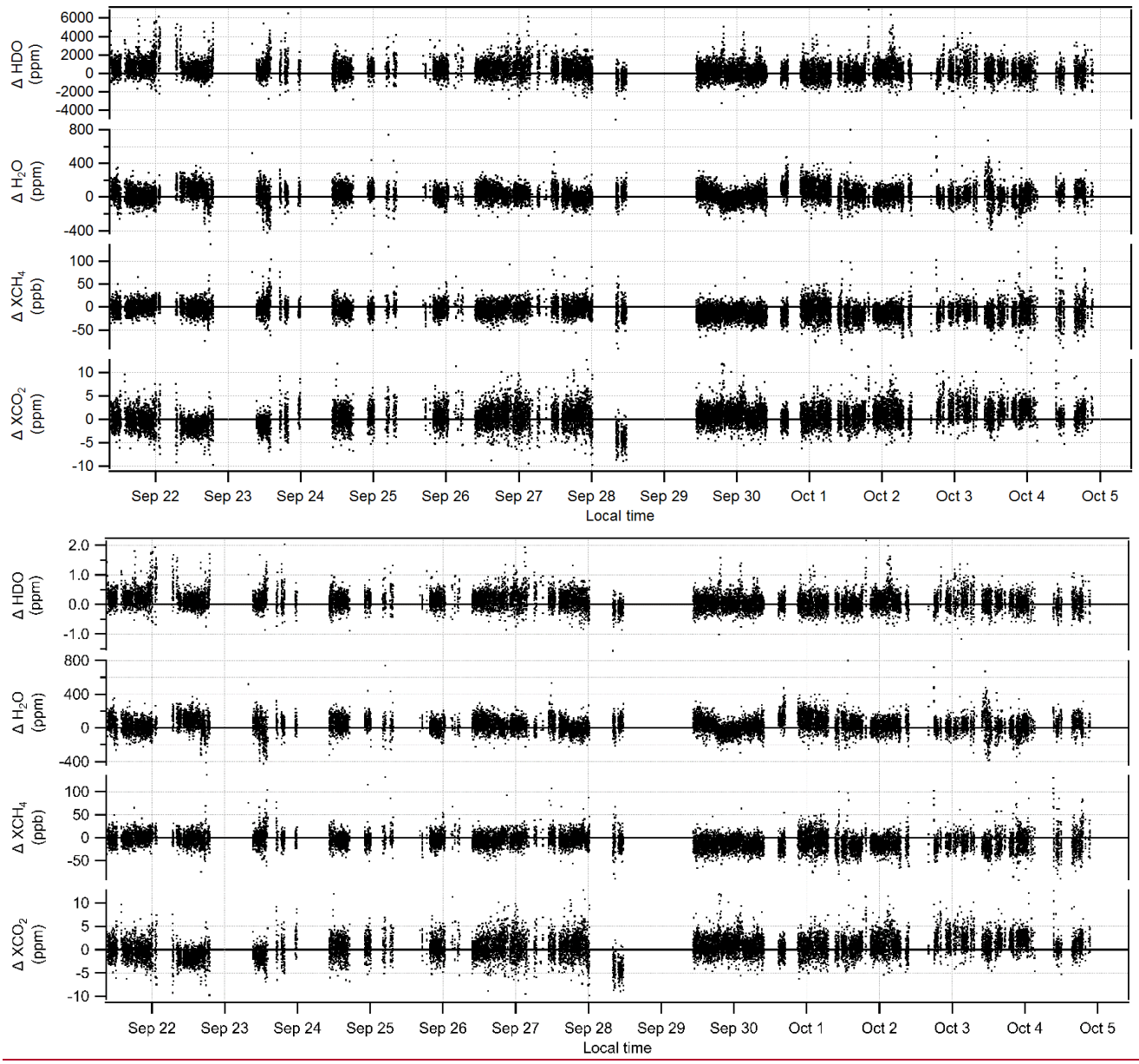

Figure 6. Time series of concentration differences, where difference is defined as DCS A - DCS B.

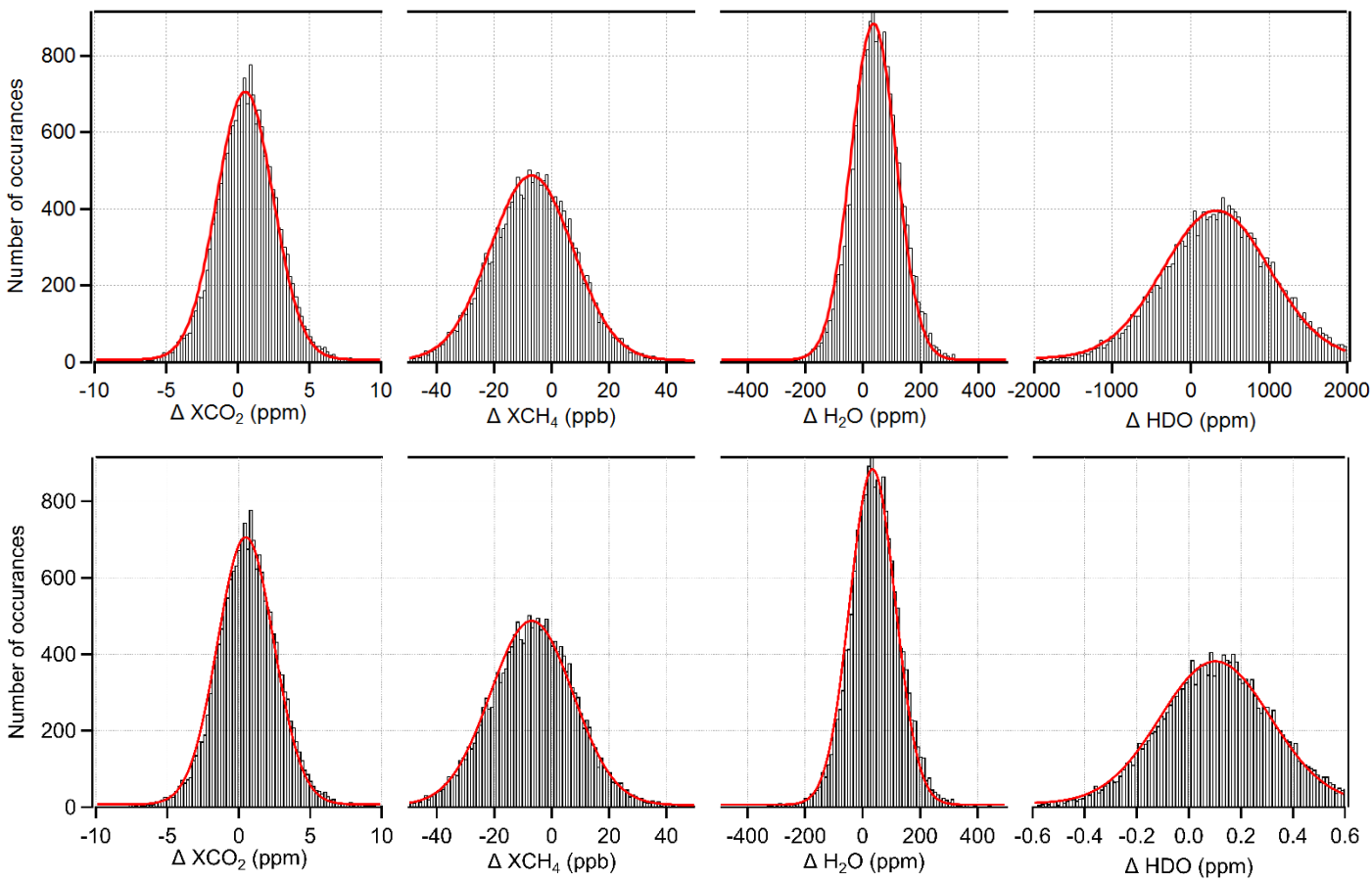

Figure 7. Statistical distributions of the differences between DCS A and DCS B for dry CO_2, dry CH_4, H_2O, and HDO from Fig. 6. Histograms are shown in black with a fit to Gaussian curves in red. These data are for ~30-second intervals; the widths are approximately halved if the data is averaged to 5-minute intervals.

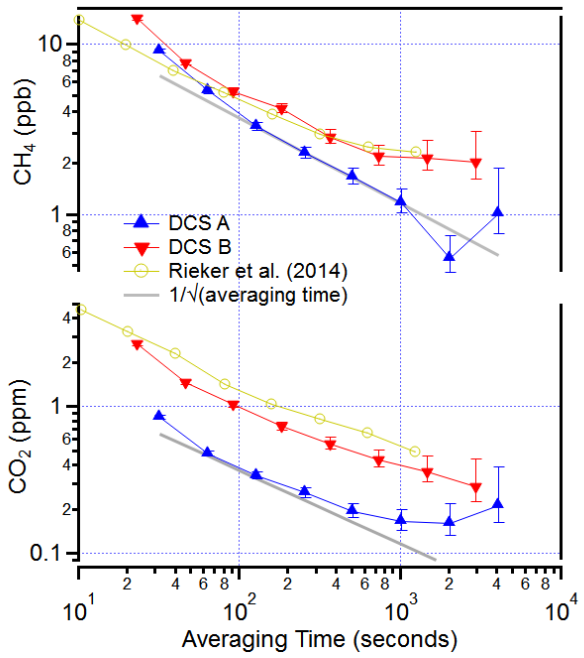

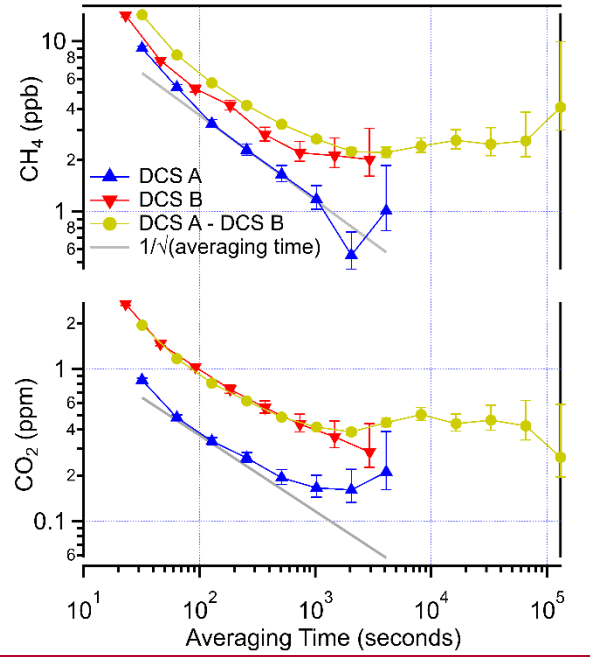

Figure 8. Precision (Allan deviation) versus averaging time, τ, for CH_4 and CO_2 ~~calculated~~ for DCS A (blue) and DCS B (red) over a 2-km path for the time period highlighted in Figure ~~3. The~~5. The improved precision of the DCS A results from higher signal-to-noise ratio of the measured spectra. The DCS B precision is slightly better than previously-published precisions from Rieker et al. (2014~~) are also shown (gold).~~). The grey line illustrates the slope expected for white noise. For DCS A, at averaging times from 30s to 1000s, the precision roughly follows ~40 ~~ppbv/$\sqrt{\tau}$ for CH4 and ~4 ppmv/$\sqrt{\tau}$ for CO_2 (gray lines).~~ $ppb/\sqrt{\tau}$ for CH4 and ~4 $ppm/\sqrt{\tau}$ for CO_2 (gray lines), where τ is in seconds, before reaching a floor near 1000 s. Also shown are the Allan deviations for the difference between DCS A and DCS B from Figure 6 (gold). These differential Allan deviations also reach a floor at ~1000 s suggesting the floor in the individual Allan deviations are due to instrument rather than atmospheric variations.

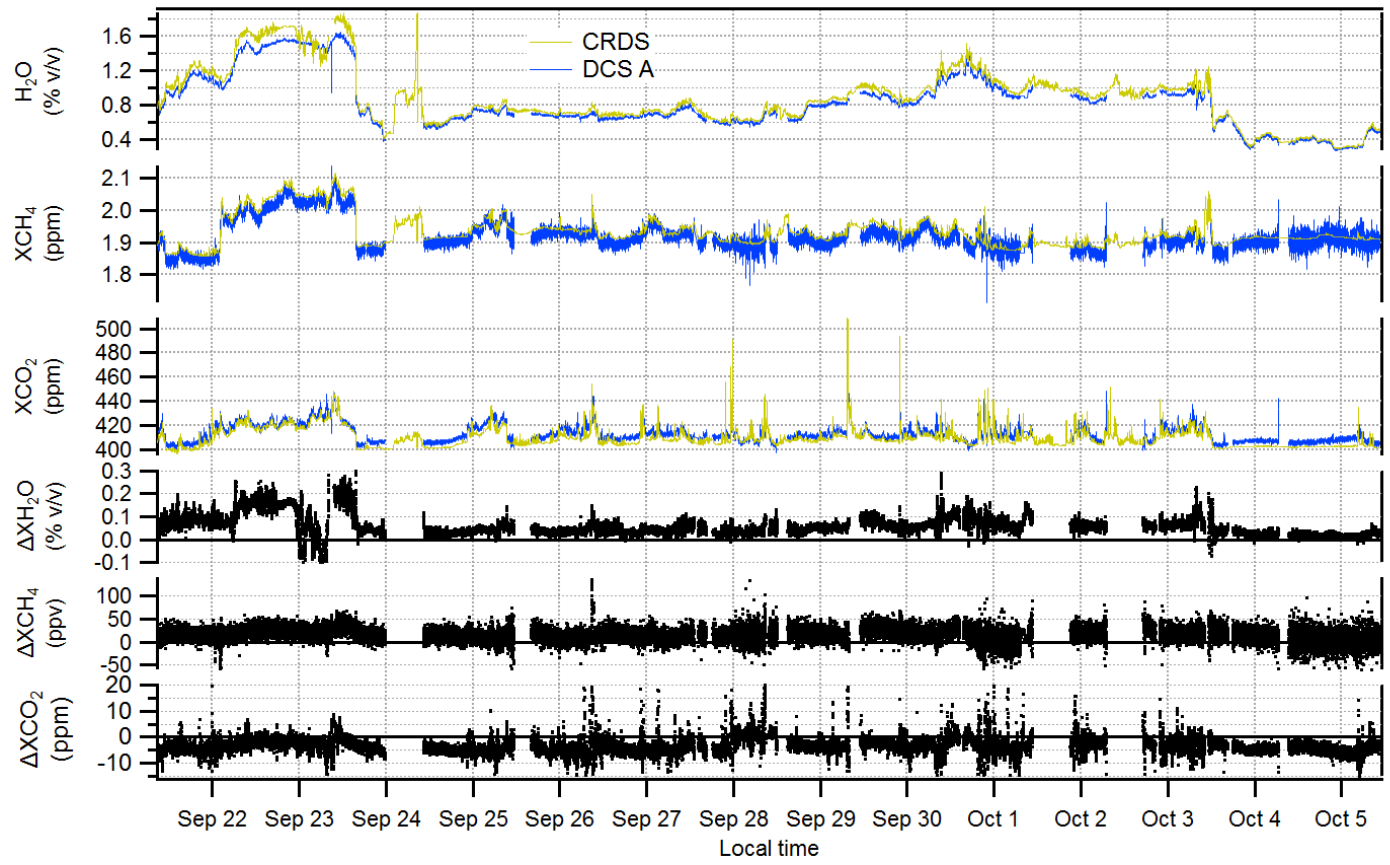
H2O (% v/v)
1.6
1.2
0.8
0.4
CRDS
DCS A
XCH4 (ppm)
2.1
2.0
1.9
1.8
XCO2 (ppm)
500
480
460
440
420
400
ΔXH2O (% v/v)
0.3
0.2
0.1
0.0
-0.1
ΔXCH4 (ppv)
100
50
0
-50
ΔXCO2 (ppm)
20
10
0
-10
Sep 22
Sep 23
Sep 24
Sep 25
Sep 26
Sep 27
Sep 28
Sep 29
Sep 30
Oct 1
Oct 2
Oct 3
Oct 4
Oct 5
Local time

755

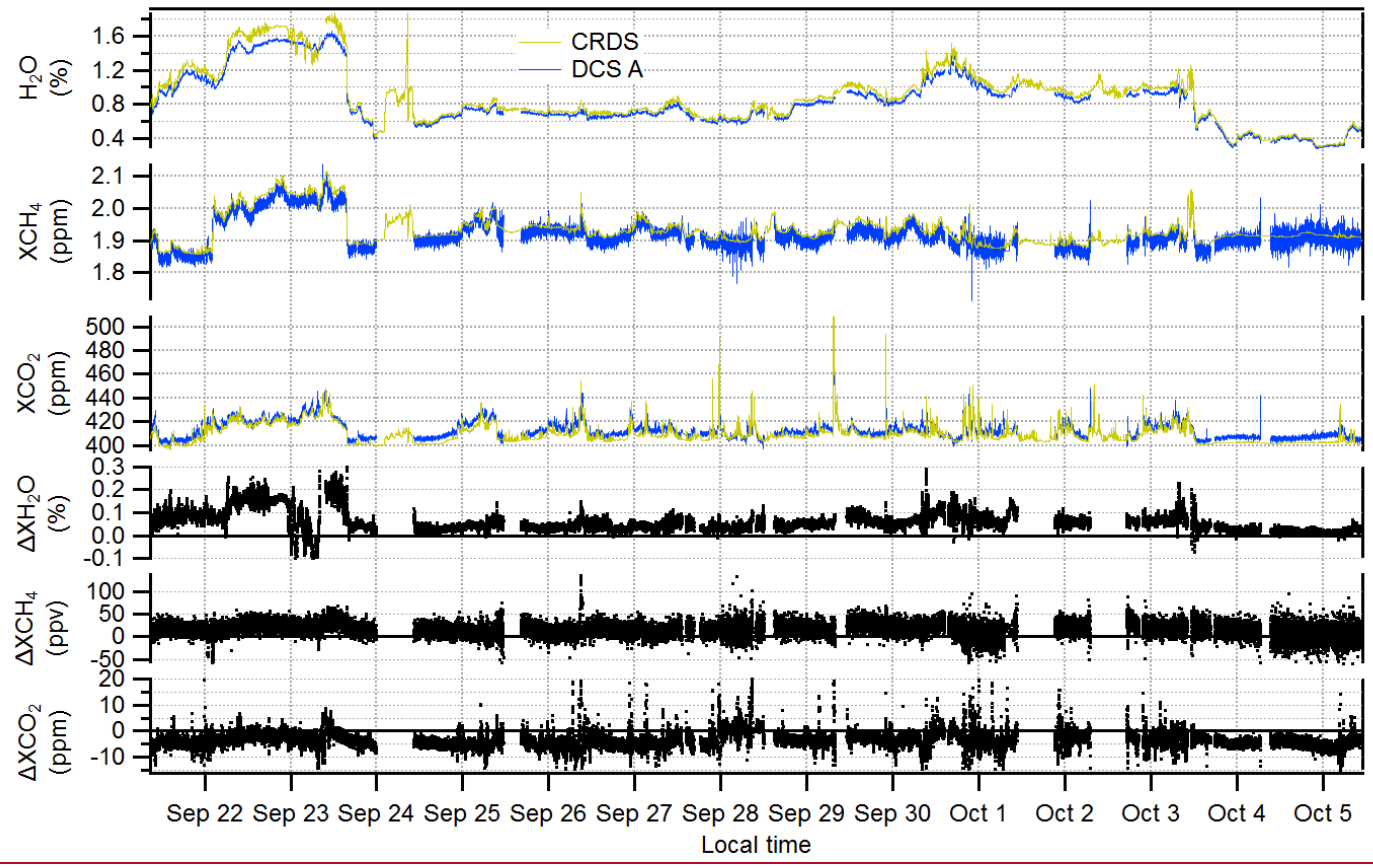

Figure 9. Comparison between the open-path DCS A data (blue) and the point CRDS data (gold) for H_2O, dry CH_4, and dry CO_2 at 32-second intervals over two weeks. The lower three panels directly plot the corresponding difference between the two.

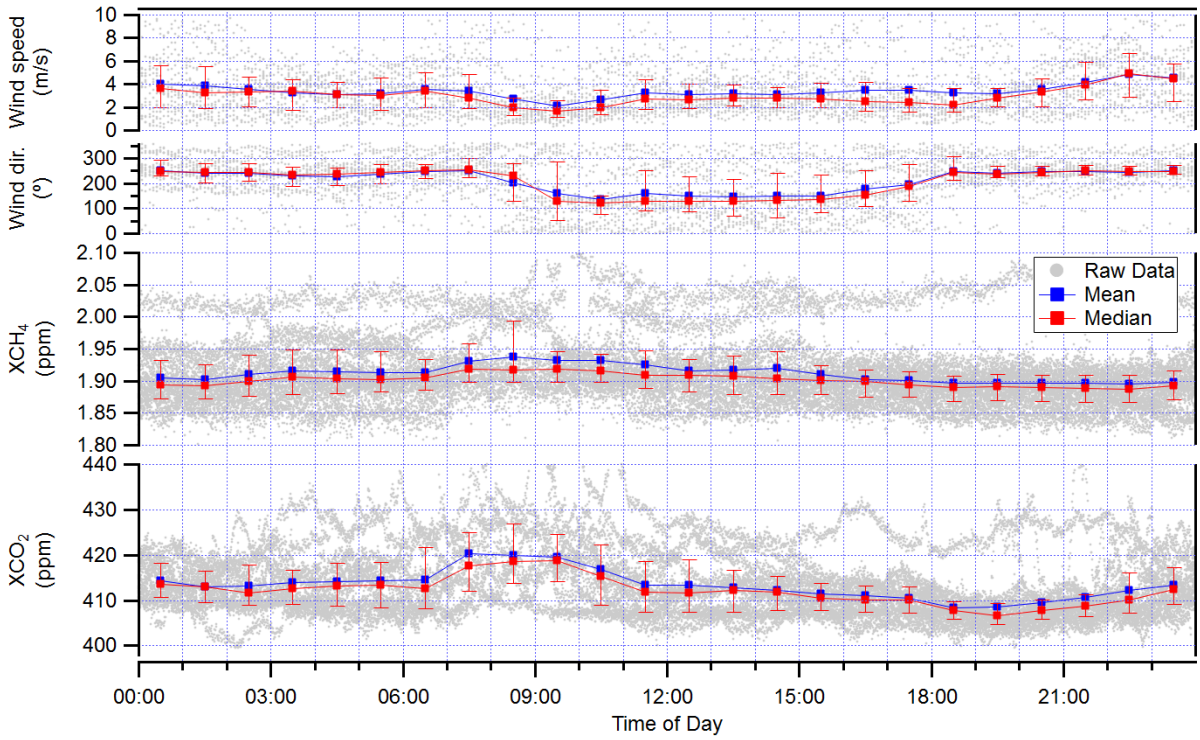

Figure 10. Diurnal cycles for wind speed, wind direction, XCH_4, and XCO_2. Data from each day in Figure 5 is over-plotted in grey along with the hourly mean (blue) and median (red) values. Uncertainty bars on the median values span the 75th quantile and 25th quantile.

Appendix A: Temperature studies

As described in Section 2.45, we extract the path-averaged temperature directly from a fit to the 30013 ← 00001 overtone band of CO_2. We perform this fit on 5-minute averages, rather than 32-second averages, under the assumption the temperature changes are still slow at that timescale. This path-averaged temperature is then used in a subsequent fit over the full spectral region to extract the column densities, and finally the mole fractions. We use a common temperature (from DCS A fit) to analyze both data sets in order to separate out instrument effects from the temperature, but the fitted temperatures between instruments show less than 0.25 °C bias.

Figure A1 compares this fitted path-averaged temperature from DCS A to three point sensors, two of which are located on the rooftop near the telescope launch point and one that is located ~ 2.2 km away at an altitude ~200 m above the overall open path. As shown in Figure A1, the two rooftop temperature sensors located near the telescope agree well with each other, but do not agree with the fitted path-averaged temperature. Moreover, that disagreement has a distinct diurnal character, supporting the argument it arises from a real temperature gradient. In contrast, the path-averaged temperature does often agree well with the temperature measured by the third temperature point sensor located at similar or higher altitude as the open path on the NCAR Mesa building (ftp://ftp.eol.ucar.edu/pub/archive/weather/mesa/). These data indicate that the point sensor located at the telescope site is not a good proxy for the path-averaged temperature; instead, the fitted path-averaged temperature should be used for the concentration fits because of temperature gradients. Note that the temperature gradients themselves do not lead to appreciable errors in the retrieved mole fractions if the correct path-averaged temperature is used (see Table 2 and Section 3.4).

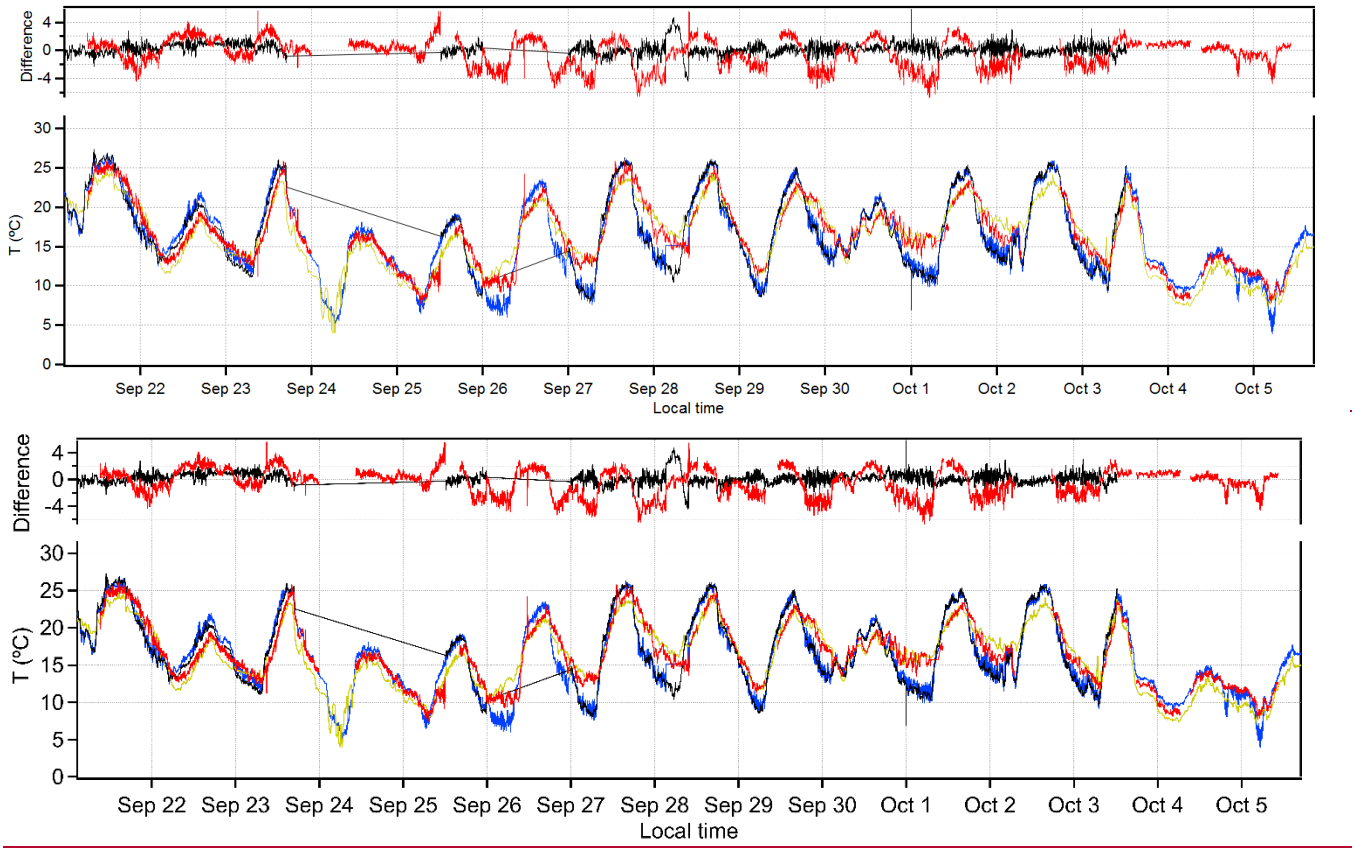

Figure A1: The fitted path-averaged temperature over two-weeks at 5 minute intervals (red) compared to the measured air temperature from a roof-top anemometer located near the telescope (blue), a second thermistor temperature sensor also located on the roof but 100-m distant (black), and a third rooftop temperature ~2.2 km distant at the NCAR Mesa facility (gold). Top panel: The difference between the two rooftop temperature (black) agree to within 1°C, but the difference between these rooftop sensors and fitted path-averaged temperature (red) shows larger 2-4°C diurnal differences, indicating it is not sufficient to measure the temperature at one "end point" of the open path. In fact, the path-averaged temperature agrees better with the more distant, but higher elevation temperature sensor located at the NCAR Mesa facility.